

# Jet Quenching in Heavy Ion Collisions

URS ACHIM WIEDEMANN

*Theory Unit, Department of Physics, CERN, CH-1211 Geneva 23, Switzerland*

*Review article prepared for the Landolt-Börnstein volume on Relativistic Heavy Ion Physics*

*Editor: Reinhard Stock*



## Contents

<b>1</b>	<b>INTRODUCTION</b>	<b>1</b>
<b>2</b>	<b>Jets in the absence and in the presence of a medium</b>	<b>3</b>
2.1	Parametric estimates relevant for embedding hard processes in the medium . . . . .	3
2.2	Jet definitions . . . . .	6
2.2.1	Jet algorithms . . . . .	6
2.2.2	Background and background fluctuations for jet reconstruction . . . . .	7
2.3	Characterizations of the intra-jet structure . . . . .	8
2.3.1	Jet event shapes . . . . .	8
2.3.2	Jet substructures . . . . .	10
2.3.3	Jet multiplicity distributions . . . . .	10
2.3.4	Jet hadrochemistry . . . . .	12
<b>3</b>	<b>Leading hadrons in the absence and in the presence of a medium</b>	<b>13</b>
3.1	Trigger biases . . . . .	13
3.2	The nuclear modification factor . . . . .	15
3.3	Triggered two-particle correlations . . . . .	17
3.4	Features in the underlying event associated to high- $p_T$ triggers . . . . .	18
<b>4</b>	<b>High-energy parton propagation in dense QCD matter</b>	<b>19</b>
4.1	Parton propagation through dense QCD matter in the eikonal formalism . . . . .	19
4.2	Gluon radiation off quarks produced in the medium . . . . .	21
4.2.1	Gluon radiation in the path integral formalism . . . . .	21
4.2.2	Qualitative features of medium-induced gluon radiation . . . . .	25
4.2.3	Multiple gluon emission . . . . .	26
4.2.4	BDMPs, Z, ASW, GLV, ... and all that . . . . .	27
4.3	Elastic interactions between projectile and medium . . . . .	28
4.4	Monte Carlo Formulations of parton propagation in the medium . . . . .	29
4.4.1	Parton shower in the vacuum . . . . .	30
4.4.2	Simulating elastic interactions . . . . .	31
4.4.3	Simulating inelastic processes . . . . .	31
4.5	Applying the AdS/CFT correspondence to in-medium parton propagation . . . . .	34

## 1 INTRODUCTION

Understanding the passage of particles through matter amounts to understanding properties of the matter through which the particles pass. This is illustrated e.g. by the Bethe-Bloch formula for the mean rate of energy loss  $-dE/dx$ . For electrically charged particles,  $-dE/dx$  depends on several properties of matter, including its atomic excitation and ionization properties and its polarizability, which can be characterized by its plasma energy [1]. In this way, the Bethe-Bloch formula provides, for instance, information about the suitability of solids, liquids and gases to serve as detector materials for characterizing the identity and energy of an impinging particle. Inverting this logic, the same medium-dependence could be used to characterize (unknown) properties of matter by measuring the energy loss of identified and well-calibrated particles. This inverse problem is of little practical relevance for the characterization of materials, whose properties are determined by the electro-dynamical interaction, and for whose characterization a broad array of other techniques exists. However, for the characterization of the strongly interacting, high-density matter produced in ultra-relativistic heavy ion collisions, alternative methods are scarce, and the study of medium-induced parton energy loss and parton fragmentation has become one of the most promising tools for a detailed characterization [2–6]. Although the tight interplay of theory and experiment has led to rapid progress in recent years, the current understanding of medium-induced parton energy loss is incomplete, and any pure review is likely to be outdated soon. As a consequence, the present article will focus mainly on the generic physics, which a complete theory of medium-induced parton energy loss should incorporate finally. The currently pursued heuristic approaches of modeling parton energy loss will be discussed only in this more general context. Their comparison to data from RHIC is reviewed in another article in this volume [7].

Relativistic heavy ion collisions have been studied experimentally in the last decades at increasing center-of-mass energies at the Brookhaven Alternating Gradient Synchrotron AGS ( $\sqrt{s_{NN}} < 5$  GeV), the CERN Super Proton Synchrotron SPS ( $\sqrt{s_{NN}} \leq 20$  GeV) and the Brookhaven Relativistic Heavy Ion Collider RHIC ( $\sqrt{s_{NN}} \leq 200$  GeV). Soon, the Large Hadron Collider LHC at CERN will study heavy ion collisions at a center-of-mass energy  $\sqrt{s_{NN}} = 5.5$  TeV, which is almost a factor 30 higher than the maximal collision energy at RHIC. Here, we focus on collisions at RHIC [8–11] and at LHC [12–14] collider energies, which produce matter at the highest energy density in the largest volume and with the longest lifetime, which can be attained in any laboratory experiment. More precisely, the initial volume is governed by the overlap of the colliding nuclei, the attained energy density exceeds the critical energy density for the phase transition to a Quark Gluon Plasma, and during its expansion the ultra-dense partonic system spends at least the first few fm/c above this critical energy density. This is a long lifetime compared to typical strong interaction times, and hence ultra-relativistic heavy ion collisions provide a unique opportunity for studying how properties of strongly interacting non-abelian partonic matter emerge from the fundamental interactions of quantum chromodynamics (QCD). But it is a lifetime far too short to test the produced system with external probes. Thus, characterization of the properties of the produced system must proceed by studying its decay products. At RHIC and even more so at LHC collider energies, partonic interactions at perturbatively large momentum transfer become abundant and the remnants of high energy partons become experimentally accessible. This gives access to a qualitatively novel class of *auto-generated hard probes* of the produced matter. The idea behind this concept is that the identity and energy of these initially produced parent partons can be calibrated independently, e.g. by the experimentally measured and perturbatively calculated yield of the hard process in proton-proton collisions, or by the measured energy of the recoiling high- $p_T$  particle, or by calorimetric measurements which suitably subtract the high-multiplicity background of the heavy ion collision. Hence, the partons produced in high- $Q^2$  processes in a heavy-ion collision may be viewed as well-identified and calibrated projectiles, which suffer medium-induced energy loss while propagating through the dense matter produced in the collision. The task is to characterize the medium-modification of the parton propagation and to relate it to fundamental properties of the produced matter. Several aspects of this challenge are characteristically different from the problem of shooting an electrically charged particle into normal matter. In particular:

1. *The projectile has a complicated time evolution even in the vacuum.*

In the standard Bethe-Bloch formula, the charged projectiles are asymptotic initial states, which can be prepared in the infinite past. They are eigenstates of the QED hamiltonian; so, in the absence of interactions with a medium, these particles do not radiate or fragment. In contrast, the partons produced in high- $Q^2$  interactions are the seeds of final state parton showers; they are highly virtual and branch in the vacuum under the QCD time evolution into multi-parton final states. As a consequence, the nature of the projectile changes as a function of the time passed since production. What matters is not only whether the projectile interacts with a target, but also when.

2. *In parton energy loss problems, initial and final states have different physical degrees of freedom.*  
For highly virtual partons, the initial stage of this fragmentation process can be accounted for perturbatively. The non-perturbative latter stage of jet fragmentation is hadronization. Fragmentation ends when hadronization is complete, since hadrons are eigenstates of the QCD time evolution. The experimentally accessible remnant of a parent parton, a.k.a. the jet, is a multi-hadron final state, and its medium-modification must be established on top of this hadronic structure. This is very different from QED, where elementary, electrically charged projectiles such as electrons or muons do not change their identity during the interaction and the medium-modification of the projectile is fully characterized by  $-dE/dx$  and by its final transverse momentum.
3. *The target is a source of momentum transfer and of color transfer, and this color must be bleached.*  
Hadronization of a final state parton shower is a dynamical color neutralization process, which bleaches colored partons into color-singlet hadrons. While a thorough dynamical understanding of hadronization is lacking, we know that this process proceeds locally in phase space. Hence, coarse features of the phase space distribution of jets can be expected to be unmodified by hadronization. But QCD is a finite resolution theory, and for sufficiently fine resolution, hadronization effects matter. Hence, while some characteristics of a jet may be sensitive solely to medium modifications which originate in the early partonic stage of the heavy ion collision, other characteristics may be sensitive to the later stage. Any color transfer between projectile and medium will affect the dynamics of hadronization and thus jet hadrochemistry.
4. *The target evolves strongly.*

From the combined analysis of soft single-inclusive hadron spectra, two-particle correlations and their azimuthal dependence, one knows that the matter produced in a heavy ion collisions expands rapidly. Thus, the highly energetic partonic projectile propagates through an environment whose energy density decreases rapidly. As we shall review below, however, parton energy loss can depend quadratically on the in-medium path length. In this case, interactions at late times are more efficient in degrading the energy of the leading partonic projectile, and in some model scenarios this can compensate completely the decreasing energy density of the expanding system. In any case, control over the geometrical extension and dynamical expansion of the produced matter is important for any quantitative comparison with data.

Up until recently, most experimental and theoretical work on parton energy loss focussed on single-inclusive hadron spectra at high transverse momenta ( $p_T > 5 - 10$  GeV). Such hadrons can be regarded as the leading fragments of parent partons and they are accompanied by a jet-like spray of sub-leading particles. However, as discussed below, requiring detection of a high- $p_T$  hadron is a significant trigger bias on jet fragmentation, and the jet-like sprays selected in this way differ strongly from samples of jets selected by calorimetric measurements. We expect that in comparison to high- $p_T$ -triggered jet-like multi-particle states, the internal structure of jets selected by 'true' calorimetric jet measurements is significantly more sensitive to properties of the medium, simply because any trigger bias of a partonic fragmentation pattern can obscure the imprints of a medium-dependence. For the purpose of this article, we draw from this the radical consequence to discuss first qualitative expectations of the medium modification of true jets, before turning to the physics of single inclusive hadron spectra and their biases, and before discussing the current state of the art in the understanding and theoretical modeling of jet

quenching.

## 2 Jets in the absence and in the presence of a medium

Hard processes are hadronic processes involving a large momentum transfer. Their medium-dependence must be established on top of a reliable baseline. The obvious baseline is the same hard process, measured in the absence of a medium, that is, in elementary hadronic interactions such as proton-proton collisions. The study of hard processes in elementary collisions is one of the most successful textbook chapters of QCD, see e.g. [15–17]. Here, we recall in an eclectic manner only those few aspects, which are of particular relevance for the following discussion of medium effects. In particular, factorization theorems ascertain that many hard processes can be factorized into the long distance physics of hadrons, which is not perturbatively calculable but processes-independent, and the short-distance physics of partons, which is process-dependent but perturbatively calculable. For single- inclusive hadron spectra in proton-proton collisions, for instance, this factorization takes the schematic form:

$$d\sigma^{p+p\rightarrow h+X} = \sum_f d\sigma^{p+p\rightarrow f+X} \otimes D_{f\rightarrow h}(z, \mu_F^2), \quad (2.1)$$

where

$$d\sigma^{p+p\rightarrow f+X} = \sum_{ij,k\dots} f_{i/p}(x_1, Q^2) \otimes f_{j/p}(x_2, Q^2) \otimes \hat{\sigma}_{ij\rightarrow f+k\dots}. \quad (2.2)$$

Here,  $\otimes$  denotes convolutions. The long-distance information is contained in the parton distributions  $f_{i/p}(x, Q^2)$  of partons  $i$  contained in the incoming proton, and in the fragmentation function  $D_{f\rightarrow h}(z, \mu_F^2)$  for a parton  $f$  to fragment into a hadron  $h$ . The hard partonic cross section  $\sigma_{ij\rightarrow f+k\dots}$  depends in general on the partonic center of mass energy, the momentum transfer  $Q$ , the renormalization scale  $\mu$ , and possibly the masses of the partons involved in the process. This partonic cross section is calculable perturbatively as a power series in the strong coupling constant  $\alpha_s(\mu)$  up to a remainder term, which is suppressed by a power of  $Q$ . The controlled computability of hadronic cross sections rests on the scale dependence of the functions in (2.1) and (2.2). This scale dependence is governed by QCD evolution equations. Physically, it emerges from the fact that the amount of parton branching, which needs to be included in the incoming parton distributions or outgoing fragmentation functions, depends on the scale, at which the hard process is interfaced with these functions.

Equation (2.2) denotes the single inclusive cross section of hard partons  $f$ , which underlies the calculation of jet cross sections. For a jet definition which can be compared to data, one needs to understand how the partons  $f$  fragment, and one requires an operational procedure which relates hadronic fragments to jets. In the present chapter, we discuss jet measurements with an emphasis on those features which are sensitive to propagation through dense QCD matter. In chapter 3, we then turn to single inclusive hadron spectra.

### 2.1 Parametric estimates relevant for embedding hard processes in the medium

**Factorization.** Does factorization apply if one embeds a hard process such as (2.1) in hot and dense QCD matter? Factorization theorems, which include the medium-modifications relevant for heavy-ion collisions, are not known. A simple parametric estimate may illustrate the reason: Let us assume that some of the partons flowing into or out of the hard process participate in a second interaction with some momentum transfer  $Q'$ . The cross section of this secondary scattering is of order  $\sim \alpha_s/Q'^2$ . Hence, medium-modifications are suppressed by powers of  $1/Q'$ . However, factorization in the sense of (2.1), (2.2) is established typically only up to terms which are power-suppressed in  $1/Q$ . Moreover, if the medium dependence results from relatively soft, small- $Q'$  secondary interactions, then the leading term in an expansion of inverse powers of  $\alpha_s/Q'^2$  may be unreliable.

For some special classes of measurements in electron-nucleus and proton-nucleus collisions, the Liu-Qiu-Sterman (LQS) formalism guarantees the extension of factorization theorems to specific medium

effects [18, 19]. The key observation in this context is that there is a parametrically dominant class of geometrically enhanced medium-effects, which is proportional to the in-medium path length and hence to  $A^{1/3}$ . These medium effects are of order  $\sim \alpha_s A^{1/3}/Q^2$ , and they are perturbatively calculable. In these cases, hadronic cross sections are known to be given up to an accuracy  $O(\alpha_s A^{1/3}/Q^2)$  by the convolution of process-independent (twist-four) parton correlation functions in the nucleus and a hard matrix element. However, the central ideas of the LQS formalism have not been shown to carry over to hadronic cross sections in nucleus-nucleus collisions.

**Localization of the hard process.** In the phenomenological praxis of heavy ion collisions, one largely bypasses the issue of factorization. One aims at constraining with experimental data the absolute yield of highly energetic partons produced within some kinematical range in a nucleus-nucleus collision, and one then proceeds to calculating the medium-modifications of the propagation and fragmentation of these partons. In this way, one circumvents first principles calculations of *absolute hadronic yields* in the presence of hot and dense QCD matter, for which factorization theorems would be needed, and one turns to the analysis of *relative hadronic yields*; the absolute yield of the produced hard partons is constrained by data rather than calculated.

**Tagged measurements** are the simplest example for this procedure. In a tagged measurement, one measures for instance a sample of photons or Z-bosons at sufficiently high transverse momentum. These gauge bosons are produced in hard processes but they carry no color charge and they thus leave the medium unattenuated. The large transverse momentum  $p_T$  implies that the hard interaction is localized within a small length scale  $\Delta x \sim 1/p_T$  and time scale  $\Delta t \sim 1/p_T$ . If this scale is much smaller than the typical length scales in the medium [which can be expected to be set by the temperature  $T \sim O(200 \text{ MeV})$  or the saturation scale  $Q_s \sim O(2 \text{ GeV})$ ],

$$\Delta x \sim 1/p_T \ll 1/T, 1/Q_s, \quad (2.3)$$

then the hard partonic production process can be expected to be unaffected by the medium. That means in particular, that the recoil transverse momentum associated with the triggered Z-boson or photon leaves the hard partonic interaction in the same partonic configuration as in a proton-proton collision. Conceptually, this turns the recoil partons of photons and Z-bosons into probes, whose initial energy is constrained kinematically on an event-by-event basis, but which can interact with the medium in their subsequent propagation. More generally, even if there is no factorization theorem which determines the rate of high energy partons produced in hard collisions, there are multiple and mutually consistent ways of selecting in nucleus-nucleus collisions data samples, for which the rate of high energy partons produced in the initial hard processes is constrained. In general, these high energy partons, after emerging from the hard interaction, propagate through the medium. To the extent to which the numerical size of the resulting medium-effects is much larger than the uncertainties in constraining the initial kinematical condition of the propagating parton, this enables a characterization of medium-modifications without relying on theoretical control over the absolute spectra of hard processes.

**Lifetime of the virtual parton.** A parton emerging from a hard interaction with high transverse momentum  $p_T$  carries an initial virtuality  $Q$ , which can be assumed to be logarithmically distributed between  $p_T$  and a lower hadronic scale. For high  $p_T$ , this virtuality is perturbatively large. According to Heisenberg's uncertainty relation, the parton will degrade its virtuality (i.e. will start evolving closer to on-shell conditions) on a time scale  $1/Q$  in its rest frame. This degradation of virtuality is achieved by multiple parton branchings and it is at the basis of the final state parton shower. Given that the time-scale  $1/Q$  is small, the question arises to what extent the final state parton shower can be altered by a medium, and to what extent a branching process will be completed prior to time scales of order  $1/T$  or  $1/Q_s$ , on which medium-effects are expected to become relevant, see eq. (2.3). In this context, it is crucial that the lifetime of the virtual parton is Lorentz-dilated in the rest frame of the medium by a gamma factor

$\sim E_{\text{parton}}/m$ , where the mass of the parton can be identified with its virtuality, so

$$\tau_{\text{virtual life}} \simeq \frac{E_{\text{parton}}}{Q^2}. \quad (2.4)$$

In the extreme case of a parton with  $E_{\text{parton}} = 100 \text{ GeV}$  and maximal virtuality  $Q^2 \simeq (100 \text{ GeV})^2$ , this time scale is  $\tau_{\text{virtual life}} = (1/500) \text{ fm}/c$ , which is much smaller than the typical wavelengths within the medium components. So, this parton can be expected to branch prior to interacting with the medium. On the other hand, if a parton with this energy has a rather small virtuality of  $Q^2 \simeq (1 \text{ GeV})^2$ , then  $\tau_{\text{virtual life}} = 20 \text{ fm}/c$ . Such a parton will not branch within the path length of the medium, except if it interacts inelastically with the medium. These numerical estimates of hadronization times are indicative of the expected order of magnitude, but may vary depending on model assumptions [20].

In general, the description of fragmentation and hadronization in elementary collisions (i.e. in the vacuum) requires momentum space information only. In contrast, the description of medium effects must also be based on a picture of how the hard process is embedded in and propagates through the spatio-temporal region over which the medium extends. Time scales of the type (2.4) determine the spatio-temporal embedding of hard processes and thus decide whether and at what stage within their fragmentation process, remnants of high energy partons emerging from a hard process will interact with the medium. We note that at least some aspects of this picture are testable. In particular, the non-perturbative stage of parton fragmentation, a.k.a. hadronization, occurs as soon as the parton shower has evolved to sufficiently low virtuality, say  $Q^2 \leq (1 \text{ GeV})^2$ . According to eq. (2.4), if at that scale in the evolution a leading parton still carries an energy of  $E_{\text{parton}} = 10 \text{ GeV}$ , then its lifetime is  $\tau_{\text{virtual life}} \simeq 2 \text{ fm}/c$ . For hadronization to occur at  $Q^2 \leq (700 \text{ MeV})^2$ , we would extract a lifetime of  $\tau_{\text{virtual life}} \simeq 4 \text{ fm}/c$ . Qualitatively, these estimates indicate that if the leading parton in a parton shower carries more than  $O(10) \text{ GeV}$  energy at the end of the perturbative evolution, then it can be expected to live long enough to hadronize outside the medium in the vacuum. Assuming that leading partons fragment into leading hadrons, this indicates that above  $p_{\perp} \geq O(10) \text{ GeV}$  medium-modifications of single inclusive hadron spectra should show the same relative hadrochemical composition as in the vacuum, since their hadronization is unaffected by the medium. This is consistent with observations of the particle-species independence of high- $p_T$  hadron suppression, made at RHIC.

**Formation time.** The process of parton fragmentation involves numerically important quantum interference effects, see section 4. As a result, the picture of a parton shower as a probabilistic iteration of parton branching processes has limitations. Interestingly, the most important interference effects can be included in a probabilistic language. In particular, there is a one-to-one correspondence which maps the destructive interference between subsequent gluon emission onto an angular ordering prescription between subsequent probabilistically iterated branchings [16, 21]. This is implemented in technically different ways in the QCD parton showers of state of the art Monte Carlo event generators [22–24].

For targets of finite spatial extension, this is not the only important quantum interference effect. If a parton branches a gluon before entering a secondary interaction, the question arises whether the two decay products should be considered as independent projectiles, or whether they scatter coherently. A simple quantum mechanical argument helpful in deciding this question is based on estimating the phase difference between the decay products. Here, the relevant phase factor in the wave function of each parton is  $\sim \exp[iE_{\perp} \Delta z]$ , where  $E_{\perp}$  is the transverse energy and  $\Delta z$  is the distance in the direction in which the projectile propagates. For instance, if a quark fragments  $q \rightarrow q g$  a gluon with energy  $\omega$  and transverse momentum  $k_T$ , then the inverse transverse energy defines the formation time

$$\tau_{\text{form}} = \frac{2\omega}{k_T^2}. \quad (2.5)$$

For  $\Delta z = \tau_{\text{form}}$ , the relative phase  $E_{\perp} \Delta z$  between the two daughter parton wave functions is unity, and that indicates decoherence of the wave function of the emitted gluon from its parent. On time scales



small compared to  $\tau_{\text{form}}$ , however, the two components of the projectile wave function can be expected to act coherently, that means, scattering proceeds as if the gluon is not yet formed, see section 4.4.3 for more details.

We note that if a virtual parton splits in the vacuum into two approximately massless daughters with momentum fractions  $z$  and  $(1 - z)$ , then the relative transverse momentum between the outgoing partons satisfies  $k_T^2 \simeq z(1 - z)Q^2$ . Taking the soft daughter parton to be the gluon with energy  $\omega = z E_{\text{parton}}$  and setting  $(1 - z) \simeq 1$ , one finds  $2\omega/k_T^2 \simeq 2 E_{\text{parton}}/Q^2$ . This shows that the estimates (2.4) and (2.5) are closely related.

## 2.2 Jet definitions

A jet is the collimated set of hadronic decay products of a parent parton. But the concept of a parton is ambiguous, for instance because it is scale dependent. As a consequence, there are different definitions of what a jet is, and these correspond to different algorithms for searching jets in hadronic collisions and - in general - they yield different results. It is hence important that the theoretical calculation of a jet matches the measurement procedure. According to the *SNOWMASS accords* [25], which were agreed on by experimentalists and theorists in 1990, a 'good' jet definition should be simple to implement in experimental analysis and theoretical calculations, it should be defined and yield finite cross sections at any order of perturbation theory, and the obtained cross sections should be relatively insensitive to hadronization. Because of the requirement on the validity of perturbation theory, the algorithm with which jets are characterized in hadronic collisions must be infrared and collinear safe, i.e., the notion of a jet should not depend upon adding or subtracting a soft particle or upon collinearly splitting a hard particle. Also, it should be as insensitive as possible to the underlying event.

There has been significant progress recently on improving jet definitions (see e.g. Ref. [26] and references therein) in line with the *SNOWMASS accords* and there are arguments that this novel generation of jet definitions should be suited for analyzing jets in the high-multiplicity environment created in heavy ion collisions. So far, essentially all high- $p_T$  data analyses at RHIC have been carried out either on the level of single inclusive hadron spectra, or by constructing jet-like particle correlations with the help of high- $p_T$  trigger particles. Only recently, a first attempt was made to use calorimetric jet definitions for the analysis of RHIC data [27]. This analysis identified calorimetric towers with a jet energy  $E_{\text{jet}} \leq 40 \text{ GeV}$ , which is large for RHIC kinematics, but which is still small compared to the energy scales at which one characterizes jets normally. These kinematical limitations at RHIC are certainly one of the reasons for why there is still little experience in applying calorimetric jet definitions to the high-multiplicity environment of heavy ion collisions. We expect that this situation will change radically with the much wider kinematic range accessible at the LHC.

### 2.2.1 Jet algorithms

Classical jet algorithms can be grouped roughly into two classes:

**Cone algorithms** aim at defining jets as dominant directions of energy flow within a circle of radius

$$R = \sqrt{(\Delta y)^2 + (\Delta \phi)^2} \quad (2.6)$$

in the  $(y, \phi)$ -plane of rapidity  $y$  and azimuth  $\phi$ . [Longitudinally invariant cone algorithms are clearly formulated in terms of rapidity rather than pseudo-rapidity  $\eta$ , but there are cone algorithms formulated in  $y$ .] The center of this cone is defined by the sum of the momenta lying in the cone. Most cone algorithms are seeded, that means that the algorithmic reconstruction of jets starts from a set of seeds which are e.g. all calorimetric towers in the  $(y, \phi)$ -plane showing more than a certain energy. The idea is then to vary the content of the cone and thus its direction, till it coincides with a local maximum of energy flow in the  $(y, \phi)$ -plane. A complication of cone algorithms is that different cones may overlap. One thus requires a prescription which either prevents the algorithm from finding overlapping cones, or which defines how to

distribute the content in the overlap of two jet cones. Both avenues have been explored in the praxis. In particular, by iteratively removing those calorimetric towers from the event, which have been attributed to a jet (iterative cone algorithms with progressive removal), one ensures that overlap does not occur. Alternatively, there are iterative procedures which amount to splitting and merging overlapping cones (cone algorithms with split-merge). A second complication is that for the simplest jet cone algorithms, the addition of an infinitely soft particle can in principle change the clustering of jets in an event. Most currently used cone algorithms have procedures implemented to control or remedy this phenomenon, but the performance of these procedures in the high-multiplicity environment of a heavy ion collision deserves further studies. There is one recently proposed cone algorithm, SISCONe [28] (Seedless Infrared-Safe Cone jet algorithm) which meets the SNOWMASS accords, that means, it is infrared and collinear safe.

From jet production at LEP, LEP2 and Tevatron, one know that for jets of energy 100 GeV, approximately 70 % of the jet energy is contained in a cone of radius  $R = 0.3$ , and approximately 90 % of the jet energy is contained in a cone of radius  $R = 0.5$ . These jet energy fractions narrow slightly with increasing jet energy, and there is a parametrization based on data from the D0-collaboration [29]. Clearly, to capture most of the jet energy, a cone radius  $R > 0.3$  is needed. In hadronic collisions, one typically uses cone radii  $0.7 < R < 1.0$ .

**Jet reconstructions based on successive recombinations.** These reconstruction algorithms are based on defining a distance  $d_{ij}$  between any pair of objects in an event as well as a so-called beam distance  $d_{iB}$  for each object. For each event, one identifies the smallest distance. If this distance is smaller than the beam distance, then one combines the two objects into one. If it is larger, then the object is called a jet and removed from the event. This is repeated till no object is left. There are essentially three successive recombination algorithms, which are infrared and collinear safe. They are defined by the distance measures

$$d_{ij} = \min(k_{T,i}^{2p}, k_{T,j}^{2p}) (\Delta y_{ij}^2 + \Delta \phi_{ij}^2), \quad (2.7)$$

$$d_{iB} = R^2 k_{T,i}^{2p}. \quad (2.8)$$

Depending on the integer  $p$ , these distances define the Cambridge/Aachen algorithm [30, 31] for  $p = 0$ , the  $k_T$  algorithm [32] for  $p = 1$  and the anti- $k_T$  algorithm [33] for  $p = -1$ .

A variant of the  $k_T$  algorithm specially suited for  $e^+ e^-$  collisions is the Durham clustering algorithm [34], where one defines for each pair of final state particles the distance

$$d_{ij} = 2 \min(E_i^2, E_j^2) (1 - \cos \theta_{ij}) / E_{\text{cm}}^2. \quad (2.9)$$

The pair of particles with smallest  $d_{ij}$  is then replaced by a pseudo-particle, whose energy and momentum are the sums of its daughters. The procedure is repeated until all  $d_{ij}$  exceed a given threshold  $d_{\text{cut}}$ .

In the above, we have focussed mainly on jet algorithms of the second generation, which meet the SNOWMASS accords. A short overview of other currently used jet algorithms is given in Ref. [26].

## 2.2.2 Background and background fluctuations for jet reconstruction

In a central Pb-Pb collision at the LHC, there is - unrelated to jet production - typically a total transverse energy per unit rapidity of  $dE_T/d\eta$  of 1 TeV or more. This estimate is obtained by multiplying the expected average  $\langle \sqrt{p_T^2} \rangle \sim 700$  MeV per hadron with a minimal multiplicity  $dN/d\eta = 1500$  of the sum of charged and neutral particles. The area  $A_{\text{jet}} = \pi R^2$  of a jet cone covers a significant fraction of the entire area  $A_{\text{total}} = \Delta\eta \times \Delta\phi = 2\pi$  within one unit of pseudo-rapidity. As a consequence, the high-multiplicity environment leads - unrelated to jet production - to an energy of

$$E_{bg}(R) > \frac{A_{\text{jet}}}{A_{\text{total}}} 1 \text{ TeV} = \begin{cases} 45 \text{ GeV} & \text{for } R = 0.3 \\ 125 \text{ GeV} & \text{for } R = 0.5 \\ 245 \text{ GeV} & \text{for } R = 0.7 \end{cases} \quad (2.10)$$

These numbers indicate that in a heavy ion collision, the transverse energy of the underlying event in a cone of typical radius  $0.3 < R < 0.7$  is comparable in magnitude to the energy added by the jet. Reducing the cone size or applying a transverse momentum cut does both reduce the background strongly whereas it affects the jet signal to a much lesser extent.

The reconstruction of the energy of a jet can be at best as accurate as the estimate of the background energy, which is contained in the same jet cone and which must be subtracted. For event-by-event jet reconstruction, this accuracy is limited by the fluctuations in the background. We distinguish two different contributions:

1. *Fluctuations caused by event-by-event variations in impact parameter*

A centrality class is a selection of events with a certain spread in multiplicity and in impact parameter. This spread translates into a fluctuation of the total background energy inside a cone

$$\Delta E_{\text{bg}}^{\text{EbyE}} \propto R^2. \quad (2.11)$$

Since the variation of impact parameter affects multiplicity inside and outside the cone in a correlated way, information from outside the cone (e.g. from other rapidity windows) can be used to estimate the effects of this fluctuation on an event-by-event basis.

2. *Out-of-cone multiplicity fluctuations in events at fixed impact parameter*

Under the assumption that the particles produced in the collision are uncorrelated, these background fluctuations are Poissonian, and their r.m.s. is (see e.g. Ref. [12])

$$\Delta E_{\text{bg}}^{\text{Poisson}} = \sqrt{N} \sqrt{\langle p_T \rangle^2 + \sigma_{p_T}^2} \propto R. \quad (2.12)$$

Here,  $N$  is the number of uncorrelated particle in the cone, and  $\sigma_{p_T}$  is the r.m.s. of the transverse momentum spectrum. However, the intermediate and high- $p_T$  particles, which dominate  $\Delta E_{\text{bg}}^{\text{Poisson}}$ , show jet-like correlations. This leads to fluctuations which are stronger than those obtained in the Poissonian limit

$$\Delta E_{\text{bg}}^{\text{real}} > \Delta E_{\text{bg}}^{\text{Poisson}} \quad (2.13)$$

Any estimate about the extent to which the Poisson assumption underestimate multiplicity fluctuations requires a dynamical understanding of jet-like correlations.

## 2.3 Characterizations of the intra-jet structure

Since jets are multi-particle final states, a large number of independent measurements has been used for their characterization. In general, these measurements characterize the energy flow, the particle distribution, particle correlations and particle identity within a jet. In the following, we discuss the most common measures.

### 2.3.1 Jet event shapes

Some of the best studied measurements of jet energy flow correspond to perturbatively calculable, infrared-safe quantities. In the context of heavy-ion physics, their study has started only recently, but it is of potential interest for several reasons. First, perturbative calculability indicates that the measurement is mainly determined by the partonic large- $Q^2$  part of the parton shower. This corresponds to very early times of order  $\sim E/Q^2$  into the parton shower evolution [see equation (2.4)], and thus any medium-modification of such measurements can be expected to be sensitive to the early and dense stage of the collision. Second, infrared-safe quantities may be easier to characterize within the high-multiplicity environment of a heavy-ion collision, since infrared safety implies a relatively weak dependence (ideally, an insensitivity) to the underlying event. Thrust  $T$ , thrust major  $T_{\text{maj}}$  and thrust minor  $T_{\text{min}}$  are amongst

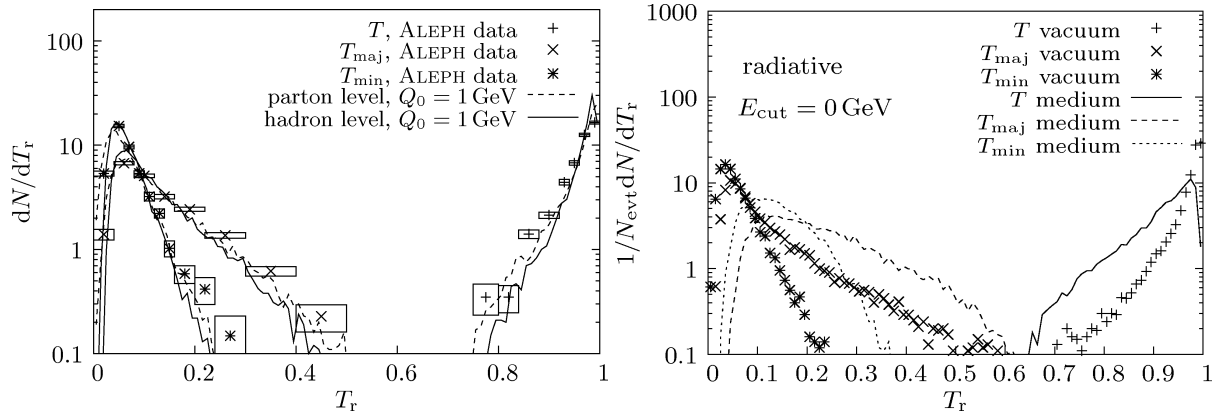


Figure 1: The thrust, thrust major and thrust minor ( $T_r = (T, T_{\text{maj}}, T_{\text{min}})$ ) distributions for jets in  $\sqrt{s} = 200 \text{ GeV } e^+e^- \rightarrow q\bar{q} \rightarrow X$  collisions. LHS: Data of the ALEPH Collaboration [35] are compared to a Monte Carlo simulation with and without subsequent hadronization. RHS: In a model, in which the medium induces additional gluon radiation, all thrust distributions broaden significantly compared to the vacuum baseline. Figures taken from Ref. [36].

the best studied perturbatively calculable, infrared-safe jet event shapes [16]. For these quantities, one sums over the three-momenta  $\vec{p}_i$  of all final state particles. According to the definition of thrust,

$$T \equiv \max_{\vec{n}_T} \frac{\sum_i |\vec{p}_i \cdot \vec{n}_T|}{\sum_i |\vec{p}_i|}, \quad (2.14)$$

a 2-jet event is pencil-like if  $T = 1$ , that is if all particles are aligned parallel or antiparallel to a thrust axis  $\vec{n}_T$ . The event is spherical if  $T = 1/2$ . Thrust major and thrust minor characterize the jet energy flow in the plane orthogonal to the thrust axis  $\vec{n}_T$ . Thrust major is defined as the projection of all particle momenta on the direction  $\vec{n}$ , which is orthogonal to  $\vec{n}_T$  and along which the momentum flow is maximal

$$T_{\text{maj}} \equiv \max_{\vec{n}_T \cdot \vec{n}=0} \frac{\sum_i |\vec{p}_i \cdot \vec{n}|}{\sum_i |\vec{p}_i|}. \quad (2.15)$$

Thrust minor sums up the components  $\vec{p}_{ix}$  of the final particle momenta  $\vec{p}_i$ , which are orthogonal to the plane defined by  $\vec{n}$  and  $\vec{n}_T$ ,

$$T_{\text{min}} \equiv \frac{\sum_i |\vec{p}_{ix}|}{\sum_i |\vec{p}_i|}. \quad (2.16)$$

The left hand side of Fig. 1 shows data from the ALEPH collaboration, compared to a Monte Carlo simulation. We note that according to perturbative QCD, the destructive interference between successive gluon emissions translates into a strong angular ordering of the parton shower. As a consequence, the first branching process in the parton shower typically carries significantly more transverse momentum (measured with respect to the thrust axis  $\vec{n}_T$ ) than subsequent branchings. This implies that the first branching largely determines thrust major. Also, the orientation of the second branching with respect to  $\vec{n}_T$  and  $\vec{n}$  significantly influences the degree to which thrust minor is more narrow than thrust major. On the level of these qualitative considerations, one sees already that thrust, thrust major and thrust minor provide a detailed test of the dynamical description of multiple parton branching processes. Moreover, since branchings at low virtualities  $Q^2$  do not result in significant transverse momenta between the daughter partons, these quantities are relatively insensitive to the "late" low- $Q^2$  stage of the parton shower and to hadronization. The right hand side of Fig. 1 illustrates that despite their perturbative calculability for elementary interactions, these event shapes show in model calculations a strong sensitivity to a class of potential medium-modifications. For instance, any interaction between the medium and the parton shower, which induces additional gluon radiation at early stages of the parton shower does leave distinct traces in thrust, thrust major and thrust minor.

The interaction of a jet with the dense QCD matter produced in heavy ion collisions can be expected to lead to a broadening of the jet energy flow, which can be characterized by jet shape observables. Characteristics of the broadening can be expected to be sensitive not only to properties of the dense QCD matter, but they will also give access to the microscopic dynamics of the interaction between probe and medium. On general grounds, for instance, elastic interactions between probe and medium (which are sometimes referred to as collisional energy loss) are dominated by small-angle scattering processes, and the degrees of freedom in the medium which accept the scattering recoil, will have low energy in comparison to the projectile partons. As a consequence elastic interactions are likely to lead to a broadening of jet shape observables, which is dominated by low- $p_T$  particles. In contrast, any medium-induced additional parton splitting tends to increase the broadening of jet event shapes by modifying the parton shower in the range of intermediate and high transverse momenta. There are by now first quantitative model studies which support this qualitative idea [36].

There is a wide class of event shape observables. It includes quantities such as oblateness, sphericity, planarity, aplanarity and total jet broadening. In principle, many of these observables are independent. In the practice of comparing Monte Carlo simulations of multi-particle final states with data, it turns out that simulations typically account satisfactorily for other event shape observables, if they account for thrust, thrust major and thrust minor. For this reason, we refer to the literature for discussion and data of other event jet observables.

### 2.3.2 Jet substructures

As discussed in section 2.2, the definition of jets depends on the distance scale with respect to which jets are defined. This distance can be a cone size  $R$ , see eq. (2.6), or a distance of the type (2.7), (2.8).

To be specific, consider the Durham cluster algorithm (2.9). The number of clusters separated by a distance larger than  $d_{\text{cut}}$  is defined to be the number  $n$  of jets. The so-called  $n$ -jet fraction measures then the number of jets in an event as a function of the resolution  $y_{\text{cut}}$ . As one decreases the resolution scale  $y_{\text{cut}}$ , a parton fragmentation pattern which has been counted as a single jet for some resolution  $y_{\text{cut}}$ , may be resolved into more than one jet. This dependence of the number of jets in an event on the resolution  $y_{\text{cut}}$  is particularly sensitive to the discrete and stochastic nature of the partonic fragmentation process.

If the interaction of a jet with the QCD matter results in additional, sufficiently energetic, medium-induced gluon radiation, then these additional partons can be expected to be seeds of additional jets at sufficiently fine resolution  $y_{\text{cut}}$ . As a consequence, one expects to count more jets at small  $y_{\text{cut}}$ . On the other hand, elastic interactions between jet and medium are unlikely to have a significant effect on the  $n$ -jet fraction, since they are dominated by small-angle scattering, which has little effect on the distance (2.9). First Monte Carlo studies support these qualitative conclusions [36].

### 2.3.3 Jet multiplicity distributions

In this subsection, we discuss mainly the understanding of inclusive single-hadron intra-jet multiplicity distributions  $dN/d\xi$ ,  $\xi = \ln[1/x]$  as a function of the logarithm of the hadron momentum fraction  $x = p/E_{\text{jet}}$  along the jet axis. These distributions can be measured for all charged hadrons, or for identified hadron species. In principle, they can also be measured separately for quark and for gluon-initiated jets. In what follows, we shall denote by  $dN/d\xi$  not only hadronic, but also partonic multiplicity distributions. Since the multiplicity in a parton shower increases during the evolution, the latter are functions of the evolution scale  $Y \equiv \ln[Q/Q_0]$ ,  $Q_0 \leq O(\Lambda_{\text{QCD}})$ .

In contrast to jet shapes, which are relatively insensitive to hadronization, one may expect that the hadronic multiplicity within a jet shows a stronger dependence on the dynamics at hadronization, since any hadronic decay process affects the hadronic yield in the final state. Remarkably, however, perturbative QCD has been used with significant phenomenological success in comparisons of the shape and hadrochemistry of inclusive single-hadron jet multiplicity distributions [37–39]. Qualitatively, this

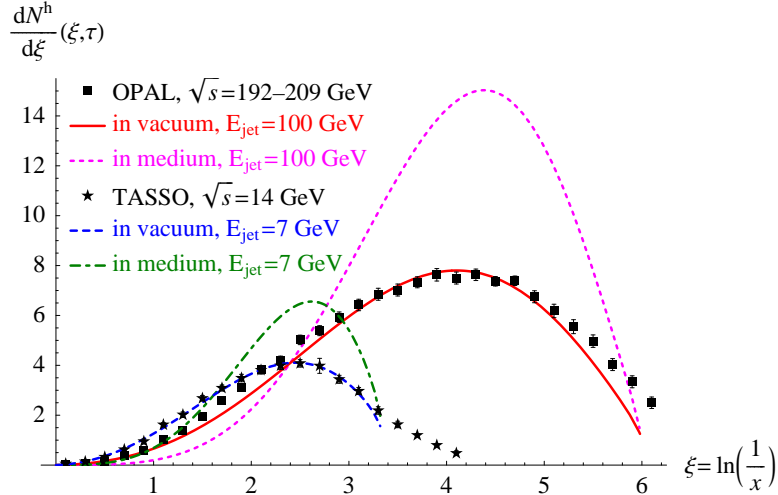


Figure 2: The single inclusive hadron distribution as a function of  $\xi = \ln [E_{\text{jet}}/p]$ . Data are taken from the  $e^+e^-$  collision experiments TASSO and OPAL,  $E_{\text{jet}} = \sqrt{s}/2$ . Lines through data denote the MLLA limiting spectrum described in the text. Dashed and dash-dotted curves labeled "in medium" are calculated for a model in which medium effects enhance gluon emission. Figure taken from [40].

may be understood as a consequence of two facts: First, hadronization becomes relevant at low virtuality. This low virtuality limits the phase space of further branching processes and hence it limit the degree to which the hadronic yield can be augmented compared to the perturbatively calculated partonic multiplicity above but close to hadronization scale. Second, there is evidence that important aspects of hadronization are local, in the sense that partonic multiplicities give rise to hadronic multiplicities within the same phase space region. Taken together, these observations support a picture, in which hadronic intra-jet multiplicity distributions can be related to partonic multiplicity distributions by an overall fit factor of order unity, which does not depend on kinematical variables. Perturbative QCD can then predict the shape and jet energy dependence of  $dN/d\xi$ .

For details of the perturbative description of jet multiplicities, we refer to the literature [37, 38]. Here, we note solely that destructive interference between soft gluon emissions within a jet is known since the early days of QCD to suppress hadron production at small momentum fractions  $x = p/E_{\text{jet}}$ . Already in the double logarithmic approximation, the QCD evolution equations in  $Y$  show the characteristic hump-backed plateau, seen in data of  $dN/d\xi$ , see Fig. 2. For a quantitatively reliable description of sufficiently small momentum fractions  $x$  and sufficiently large jet energies, where  $\ln [1/x] \sim \ln [E/Q_0] \sim \mathcal{O}(1/\sqrt{\alpha_s})$ , however, one must take into account terms of relative order  $\sqrt{\alpha_s}$ . This is achieved in the modified leading logarithmic approximation (MLLA), which provides an analytically controlled calculation in the region of sufficiently large  $\xi$ , only. Supplementing this partonic MLLA calculation [37, 38] with the hypothesis of local parton hadron duality (LPHD) [39] results in a good agreement with the jet multiplicity distributions observed in elementary collisions, see e.g. Fig. 2.

While MLLA accuracy per se is not sufficient to describe the inclusive single-hadron distribution as a function of the transverse momentum with respect to the jet axis, this is possible in a recent approach called NMLLA [41, 42], in which some parametrically higher-order terms are kept. Physically, these terms amount to improving energy momentum conservation at each parton branching. Exact energy conservation combined with MLLA accuracy can be achieved by numerical techniques [43] and appears to be quantitatively important in most of the  $Y$ - and  $\xi$ -range explored experimentally so far.

The presence of dense QCD matter produced in a heavy ion collision is expected to degrade the energy of the most energetic partons in the shower. Since the jet energy is conserved, a reduction in the energy of the most energetic partons within a jet implies an increase in the total jet multiplicity. Figure 2

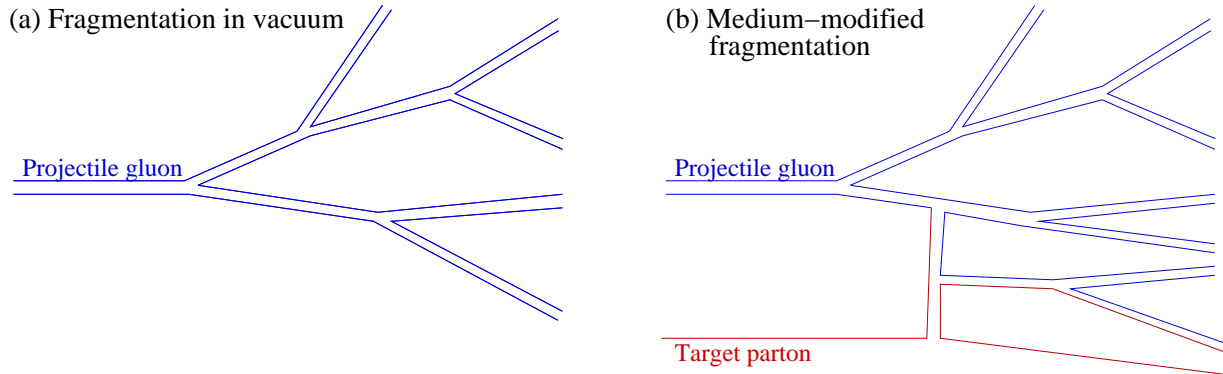


Figure 3: Sketch of an entirely gluonic parton shower in the large  $N_c$  limit, where gluons are represented as pairs of  $q\bar{q}$  fermion lines, and quarks as single lines. (a) Fragmentation of the gluon in the vacuum. (b) Interaction of the gluon with a target quark in the medium via a single gluon exchange. This interaction changes the color flow and may affect hadronization, see text. Figure taken from Ref. [46].

shows a model study which illustrates this phenomenon for the case of medium-induced additional gluon splitting. Most generally, one expects that the yield of high energy partons (small  $\xi$ ) decreases while the yield of partons of lower energy (large  $\xi$ ) increases. Assuming local parton hadron duality, this should be reflected directly in the hadronic distribution. One also expects that the multiplicity distribution broadens in transverse momentum space due to multiple scattering.

#### 2.3.4 Jet hadrochemistry

From a general perspective, highly energetic partons propagating through a dense plasma can be viewed as probes, which are initially very far away from the equilibrium state of the surrounding matter. By interacting with the medium, they participate in equilibration processes, which can be characterized by studying the medium-modification of jets. The measurements discussed so far allow us to characterize kinetic aspects of equilibration. In contrast, jet hadrochemistry addresses the question to what extent the jet embedded in the medium participates in hadrochemical equilibration processes. The sensitivity of hadrochemical jet measurements arises from the fact that the hadrochemical composition of jets in the vacuum is known to differ characteristically from that of the bulk hadronic composition in heavy ion collisions [44]. It also differs from the hadrochemical composition in RHIC heavy ion collisions at intermediate transverse momentum, which seems to follow quark counting rules [45].

From the previous subsection, we know that important qualitative and quantitative features of jet multiplicity distributions can be accounted for by perturbation theory. In particular, supplementing MLLA [37, 38] with LPHD [39] amounts to extending the perturbative shower evolution down to  $\Lambda_{\text{QCD}}$  and then assuming a one-to-one correspondence between partonic and hadronic degrees of freedom. For jets in elementary collisions, this hadronization prescription has been applied successfully to jet hadrochemistry. By evolving the parton shower for different hadron species down to scales set by the hadron masses, one can account for the main characteristic differences in the hump-backed plateaus of pions, kaons and protons. If this hadronization assumption persists in the presence of a dense QCD matter, then it leads to specific predictions for the medium-modified hadrochemical composition of quenched jets [46].

However, several other dynamical mechanisms are conceivable, which may affect the hadrochemistry of jets in the medium considerably. In particular, as sketched in Fig. 3, any gluon exchange between the parton shower and the medium changes the color flow. Since hadronization must implement color neutralization, this can change significantly the hadrochemical composition of jet fragments. In particular, for the case of a hadronization model based on string fragmentation, Fig. 3 illustrates clearly that the initial invariant mass distribution of strings may be expected to be rather different from that in the

vacuum. One may also speculate on other mechanisms. For instance, if components of the medium are kicked by the parton shower to sufficiently high transverse momentum, then the hadrochemical composition of what is kicked can affect jet hadrochemistry. We expect that jet hadrochemistry will be characterized in detail within the LHC heavy ion program.

### 3 Leading hadrons in the absence and in the presence of a medium

At sufficiently high transverse momentum, inclusive single-hadron spectra in proton-proton collisions can be calculated within the perturbative QCD factorized formalism, as discussed shortly in the context of equations (2.1) and (2.2). The qualitative discussion of length scales and time scales in section 2.1 applies to high- $p_T$  inclusive hadron spectra, as well. In particular, high- $p_T$  hadrons result from highly energetic partons, which have evolved in the parton shower down to a hadronic virtuality  $Q_{\text{hadr}}$ . The lifetime of these partons can be estimated according to (2.4) to be of the order  $E_{\text{parton}}/Q_{\text{hadr}}^2$ , which takes values of the order of a nuclear radius for  $E_{\text{parton}} \simeq 10$  GeV and typical hadronization scales. The far-reaching consequence of this parametric estimate is that for sufficiently high transverse momentum, leading hadrons form outside the medium. Thus, the medium-modification of high- $p_T$  inclusive hadron spectra is expected to be sensitive solely to the medium-modification of parton propagation, and should not depend on the interaction of hadronized fragments with the medium. An important test of this conclusion is to verify that the particle-species dependence of medium-modifications is trivial, i.e., that it arises solely from differences in the medium-modification of the parent gluons, light quarks and heavy quarks.

#### 3.1 Trigger biases

Hadronic measurements select classes of partonic fragmentation patterns. Depending on the measurement, this selection can show a significant bias. These trigger biases can be seen clearly, for instance, on the level of the average momentum fraction  $\langle z \rangle$ , which is carried by the most energetic hadron inside the experimentally selected partonic fragmentation patterns.

**Trigger bias in the vacuum.** The calculation of single inclusive spectra proceeds by convoluting the probability  $D_{f \rightarrow h}(z) dz$  of a parton  $f$  of transverse momentum  $p_T$  to fragment into a hadron  $h$  of momentum fraction  $z = p_T^h/p_T$  with the probability  $\frac{d\sigma^{p+p \rightarrow f+X}}{dp_T} dp_T$  of producing a parton with this momentum. Let us approximate the partonic cross section by a power-law  $\frac{d\sigma^{p+p \rightarrow f+X}}{dp_T} \propto \frac{1}{(p_T)^n}$ . It then follows from the hadronic cross section  $d\sigma^{p+p \rightarrow h+X} = \frac{d\sigma^{p+p \rightarrow f+X}}{dp_T} dp_T D_{f \rightarrow h}(z) dz$  that its dependence on hadronic momentum  $p_T^h$  is determined by the  $(n-1)$ -th moment of the fragmentation function

$$\langle z \rangle_{\text{lead.hadr.}} \simeq \int z^{n-1} D_{f \rightarrow h}(z) dz . \quad (3.1)$$

Within the kinematical ranges tested at RHIC and at the LHC, the hard partonic cross section is significant steeper than the  $n = 4$  dependence expected of lowest order perturbative parton-parton scattering (which should be valid in the limit  $p_T \rightarrow \infty$  with  $s/p_T^2 = \text{fixed}$ ). One of the main reasons for this steeper fall-off of  $\frac{d\sigma^{p+p \rightarrow f+X}}{dp_T}$  with increasing  $p_T$  is the  $x$ -dependence of the parton distribution functions entering (2.2). These decrease with increasing transverse parton momentum  $p_T$ , since  $x_1, x_2 \propto \sqrt{p_T^2/s}$ . There are also other effects, for instance, the running of the coupling constant  $\alpha_s(p_T^2)$  in the hard parton-parton interaction adds to increasing the power  $n$ . Clearly, for quantitative statements about the  $p_T$ -dependence of  $\frac{d\sigma^{p+p \rightarrow f+X}}{dp_T}$ , one should turn to a reliable perturbative calculation. For the purpose of this argument, however, it is sufficient to note that one has  $n \geq 7$  over a wide kinematical range at RHIC and at the LHC.

Let us contrast the measurement of a single-inclusive hadron spectrum with a measurement, in which one selects a set of events containing partons  $f$  of known transverse momentum  $p_T$ . In fact,



calorimetric jet measurements aim at selecting such an ideal event sample by measuring jets with energy  $E_{\text{jet}} = p_T$ . According to the definition of a fragmentation function, the most energetic hadron in these jets carries an average momentum fraction

$$\langle z \rangle_{\text{jet}} \simeq \int z D_{f \rightarrow h}(z) dz. \quad (3.2)$$

By comparing equations (3.1) and (3.2), one finds that single inclusive hadron spectra amount to a dramatic trigger bias, since the  $(n - 2)$ -nd moment of the fragmentation function will lie at much larger momentum fractions than its first moment (3.2). To be specific: in an  $E = 100$  GeV jets, measured at LEP2 and initiated by light quarks (up, down, strange), the leading hadron typically carries a momentum fraction of  $\langle z \rangle_{\text{jet}} \sim 1/4$ . In contrast, leading hadrons tend to carry a momentum fraction of the order of  $\langle z \rangle_{\text{lead.hadr.}} \sim 3/4$ . The difference in these average  $z$ -values indicates the numerical importance of trigger biases.

To sum up: if one requires single hadrons with momentum  $p_T^h$  (trigger condition), then the yield of such hadrons will be dominated by biased fragmentation processes in which the parent parton loses as little energy as possible into the production of subleading hadrons. This is so, since high- $p_T$  partons are rare, and the bias on the fragmentation pattern will be more severe for larger values of  $n$ , when high- $p_T$  partons are rarer.

[We note as an aside that while equations (3.1) and (3.2) are useful for illustrating the above argument, they remain schematic since we do not specify here the kinematical boundaries of the  $z$ -integration, and we do not specify the dependence of the fragmentation functions on the evolution scale, which may be different for (3.1) and (3.2).]

**Trigger biases in the medium.** Let us assume that a highly energetic parton, produced in a hard partonic process  $\frac{d\sigma^{p+p \rightarrow f+X}}{dp_T}$ , loses with probability  $P(\epsilon)$  a fraction  $\epsilon$  of its initial momentum due to the presence of the medium, prior to hadronizing outside the medium. The average medium-induced fractional energy loss of such partons is

$$\left( \frac{\Delta E}{E} \right)_{\text{average}} = \int d\epsilon \epsilon P(\epsilon). \quad (3.3)$$

However, in close analogy to the discussion of trigger biases in the vacuum, the medium-modification of the partonic cross section will be [47]

$$\frac{d\sigma^{\text{med}}(p_T)}{dp_T^2} = \int d\epsilon P(\epsilon) \frac{d\sigma(p_T/\epsilon)}{dp_T^2} \quad (3.4)$$

If the partonic cross sections falls like  $\propto 1/p_T^n$ , then the medium-modified partonic cross section will be sensitive to the typical energy loss

$$\left( \frac{\Delta E}{E} \right)_{\text{typical}} = \int d\epsilon \epsilon^n P(\epsilon). \quad (3.5)$$

The typical energy lost by the parent parton of a triggered high- $p_T^h$  hadron is much smaller than the average energy lost by parent partons of the same momentum. For a partonic cross section which is steeply falling in  $p_T$ , the measured high- $p_T^h$  hadrons are those which got away with the least medium-induced energy loss.

The probability  $P(\epsilon)$  of medium-induced parton energy loss depends on properties of the medium. In particular, it increases with increasing in-medium path length. We recall that in heavy ion collisions, there will always be an outer region of the collision, from which particles can propagate into the vacuum after little or no interaction with the medium. Since single-hadron spectra are dominated by hadrons which emerge with less than average medium-induced energy loss, this implies that the hadrons selected experimentally by measuring a single-inclusive cross section, were produced predominantly in the outer

parts of the collision region. The measured spectrum has a **surface bias** [48]. This may limit the ability of testing the medium with single inclusive hadron spectra [49], simply since the sample of hard processes selected by measuring single inclusive hadrons cannot be embedded deeply into the medium, and since the surface bias induces additional uncertainties in analyzing the medium modification.

There are several proposals to bypass this surface bias and to characterize the medium-modification of hard processes which were deeply embedded in the medium. In principle, jet measurements, based on the calorimetric measurement of jet energy flow within the high-multiplicity environment of a heavy ion collision, are independent of the surface bias (and other trigger biases), since the energy of the initial parton is conserved throughout the medium-modified parton evolution. Another promising approach to bypass surface bias effects is the study of the recoil measured in the direction opposite to a high- $p_T$  trigger particle. In this case, the fragmentation pattern on the side of the trigger particle is biased, of course, but the recoil distribution can be expected to show little bias. By now, several studies address the question to what extent triggering on photons,  $Z$ -bosons or high- $p_T$  hadrons provides sufficiently accurate calorimetric information about the recoil.

The surface bias is by far the best known, but possibly not the only qualitatively novel trigger bias, which arises in the high energy collision of heavy nuclei. For instance, one often expects that in nucleus-nucleus collisions the incoming partons can pick up transverse momentum by multiple scattering prior to entering a hard process. In this case, triggering on a single high- $p_T$  hadron will preferably select processes for which the center of mass of the hard interaction moves in the direction of the triggered particle. While this effect should be small at sufficiently high transverse momentum, it may play an important role in the region of the Cronin peak.

### 3.2 The nuclear modification factor

In the absence of medium effects, the high- $p_T$  particle yield grows proportional to the number of hard partonic interactions, which is proportional to the number of nucleon-nucleon collisions,

$$\frac{dN^{AB \rightarrow h}}{d^2p_T dy} = \langle N_{\text{coll}}^{AB} \rangle \frac{dN^{pp \rightarrow h}}{d^2p_T dy}, \quad \text{without medium effects.} \quad (3.6)$$

Here, the average number  $\langle N_{\text{coll}}^{AB} \rangle$  of equivalent nucleon-nucleon collisions in a collision between nuclei  $A$  and  $B$  is determined by a Glauber model calculation. The single inclusive spectrum  $dN/d^2p_T dy$  in a nucleon-nucleon collision is determined either experimentally (e.g. in p+p collisions at RHIC or LHC), or theoretically within the framework of perturbative factorization. To characterize deviations from this benchmark, one introduces the nuclear modification factor

$$R_{AB}^h(p_T, y, \text{centrality}) = \frac{\frac{dN_{\text{medium}}^{AB \rightarrow h}}{dp_T dy}}{\langle N_{\text{coll}}^{AB} \rangle \frac{dN_{\text{vacuum}}^{pp \rightarrow h}}{dp_T dy}}. \quad (3.7)$$

This nuclear modification factor characterizes the medium-modification of single inclusive spectra fully. By construction, it equals unity in the absence of medium-effects, and it decreases if the medium suppresses the production of hard particles.

**The nuclear modification factor at RHIC** Fig. 4 shows data for the nuclear modification factor  $R_{AA}$  at RHIC. With increasing centrality, the high- $p_T$  yield of neutral pions decreases significantly in comparison to the benchmark expectation (3.1). For the most central collisions, this suppression is approximately 5-fold. In contrast, high- $p_T$  photons appear to be unaffected within errors. This is consistent with the picture that the strong medium-induced suppression of high- $p_T$  hadrons is a final state effect, which does not occur for photons since these do not interact hadronically. Moreover, if one assumes that high- $p_T$  photon spectra remain unmodified, then the nuclear modification factor for photons becomes a test of the assumption that hard processes in heavy ion collisions scale with the number of binary nucleon-nucleon collisions, which can be determined via a Glauber calculation of  $\langle N_{\text{coll}}^{AB} \rangle$ .

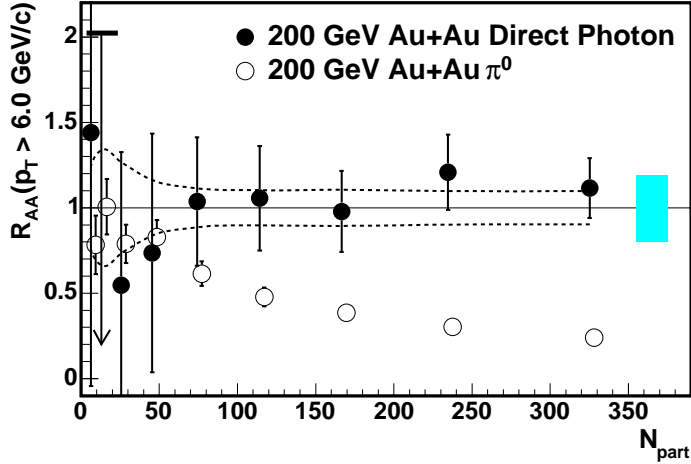


Figure 4: The nuclear modification factor (3.2) as a function of centrality given by the number of participants  $N_{\text{part}}$  for direct photons and neutral pions, measured in  $\sqrt{s_{NN}} = 200$  GeV hadronic collisions at RHIC. Particle yields are integrated above  $p_T \geq 6$  GeV. The p+p direct photon yield is taken from a next-to-leading order pQCD calculation with scale uncertainty indicated by the shaded bar on the right. Dashed lines indicate the error in determining  $\langle N_{\text{coll}}^{AB} \rangle$  in (3.2). All other errors are included in the error bars. Figure taken from Ref. [50].

Fig. 4 is but one manifestation of a generic phenomenon. In heavy ion collisions at RHIC, *all* single inclusive hadron spectra are suppressed by comparable large suppression factors. In particular, one observes [8–11] :

- *Strong and apparently  $p_T$ -independent suppression of  $R_{AA}$  at high  $p_T$ .*  
In  $\sqrt{s_{NN}} = 200$  GeV, 5-10% central Au-Au collisions at mid-rapidity, one observes a suppression of high- $p_T$  single inclusive hadron yields by a factor  $\sim 5$ , corresponding to  $R_{AuAu}^h(p_T) \simeq 0.2$  for  $p_T \geq 5 - 7$  GeV/c. Within experimental errors, this suppression is  $p_T$ -independent for higher transverse momenta in all centrality bins.
- *Evidence for final state effect.*  
For the most peripheral centrality bin, the nuclear modification factors measured at RHIC are consistent with the absence of medium-effects in both nucleus-nucleus ( $R_{AA} \sim 1$ ) and deuterium-nucleus ( $R_{dAu} \sim 1$ ) collisions. With increasing centrality,  $R_{AA}$  decreases monotonically. In contrast, no such suppression is seen in d-Au collisions. These and other observations indicate, that the suppression occurs on the level of the produced outgoing partons or hadrons, that it increases with increasing in-medium pathlength in the final state, and that it is hence absent in d-Au collisions, where the in-medium pathlength is negligible.
- *Independence of  $R_{AA}$  on hadron identity.*  
For transverse momenta  $p_T \geq 5 - 7$  GeV/c, all identified hadron spectra show a quantitatively comparable degree of suppression. There is no particle-species dependence of the suppression pattern at high  $p_T$ . Since cross sections for different hadron species differ widely, the species-independence of high- $p_T$   $R_{AA}$  indicates that the mechanism responsible for suppression occurs prior to hadronization.

We emphasize that the suppression of  $R_{AA}$  for hadrons is one of the strongest medium-modifications observed in heavy ion collisions at RHIC, and that it is a generic phenomenon found in all high- $p_T$  hadron spectra and persisting up to the highest transverse momenta or  $O(20)$  GeV measured at RHIC. The strength and  $p_T$ -independence of this phenomenon supports the view that high- $p_T$  hadron suppression will persist at LHC to much higher transverse momentum. Moreover, the above observations suggest to base a dynamic understanding of high- $p_T$  hadron suppression on the medium-induced energy loss of high energy final state partons prior to hadron formation. As a consequence, the standard modeling of

single inclusive hadron spectra proceeds by supplementing a pQCD factorized formalism (2.1) for single inclusive spectra with a medium modification of the produced partons prior to hadronization in the final state, schematically

$$d\sigma_{(\text{med})}^{AA \rightarrow h+X} = \sum_f d\sigma_{(\text{vac})}^{AA \rightarrow f+X} \otimes P_f(\Delta E, L, \hat{q}) \otimes D_{f \rightarrow h}^{(\text{vac})}(z, \mu_F^2). \quad (3.8)$$

Here, the model-dependent input is in the probability  $P_f(\Delta E, L, \hat{q})$  of losing a fraction  $\Delta E$  of the parton energy while propagating over a path-length  $L$  inside a medium characterized by properties such as the quenching parameter  $\hat{q}$ . Experimental data from RHIC are reproduced in models, which calculate  $P_f(\Delta E, L, \hat{q})$  for mechanisms of medium-induced radiative energy loss and which take the nuclear geometry properly into account [20, 49, 51–53]. Some models also identify a non-negligible role for parton energy loss via elastic interactions [54]. For a review of comparisons of these models to RHIC data, see Ref. [7, 55].

### 3.3 Triggered two-particle correlations

Triggered two-particle correlations are measurements, in which a trigger hadron of high transverse momentum  $p_T^{\text{trig}}$  is correlated with an associated hadron of momentum  $p_T^{\text{assoc}}$ . As a function of azimuthal angle  $\Delta\phi$ , there are two qualitatively distinct classes of measurements:

**Triggered near-side two-particle correlations.** A measurement of two sufficiently high- $p_T$  hadrons, which are close in  $\Delta\eta$  and  $\Delta\phi$  characterizes two particles from the fragmentation pattern of the same parent parton (assuming that there are no issues with background subtraction). However, triggered hadrons select highly biased fragmentation patterns, in which  $p_T^{\text{trig}}$  carries  $O(3/4)$ -th of the total energy of the parent parton, see section 4.1. As a consequence, also the distribution of associated hadrons is strongly biased.

In Au-Au collisions at RHIC, the yield of high- $p_T$ -trigger particles decreases by a factor 5 from peripheral to central collisions, in accordance with the measured nuclear modification factor. However, the yield,  $\Delta\phi$ -width and charge correlation in triggered near-side two-particle correlations is insensitive to the centrality of Au-Au collisions and coincides with the measurement in d-Au collisions [56, 57]. These data are consistent with the picture of an extreme surface bias, according to which high- $p_T$  triggers select those parent partons, whose fragmentation pattern is unmodified by the medium.

We are not aware of any study to what extent this surface bias could be overcome at the LHC by triggering on significantly higher transverse momenta than the high threshold trigger  $8 \text{ GeV} < p_T^{\text{trig}} < 15 \text{ GeV}$  used at RHIC. However, since a high- $p_T$  trigger on a steeply falling distribution will always select those particles which got away with the least energy loss, it is conceivable that the qualitative features observed at RHIC remain unchanged. At present, there is no compelling argument that triggered near-side two-particle correlations are sensitive to medium effects which are not yet characterized by the nuclear modification factor.

**Triggered away-side two-particle correlations.** Such measurements are expected to characterize correlations between the most energetic leading hadron of a parent parton, and the most energetic hadronic fragment of the recoiling parent parton. The triggered hadron will be associated to a strongly trigger-biased fragmentation pattern. However, if one does not apply cuts to  $p_T^{\text{assoc}}$ , the recoiling particles may be expected to emerge from an unbiased fragmentation pattern of the recoil parton.

For intermediate  $p_T$  triggers ( $4 \text{ GeV} < p_T^{\text{trig}} < 6 \text{ GeV}$ , data for Au-Au collisions at RHIC show that the associated particle yield for  $p_T^{\text{assoc}} > 2 \text{ GeV}$  disappears as a function of centrality. If the trigger threshold is raised to higher values ( $8 \text{ GeV} < p_T^{\text{trig}} < 15 \text{ GeV}$ ), the backside particle reappears again, but with strongly decreased yield. On a qualitative level, this demonstrates that by triggering on a high- $p_T$  particle, one can embed the recoil in such a way, that it is sensitive to the medium. On the other hand, the azimuthal distribution of recoiling hadrons associated to high- $p_T$  triggers does not show characteristic

medium-effects, such as broadening [57]. This may be due to the fact that azimuthal broadening is very weak. However, it might also indicate a surface bias, according to which the medium effect on the recoil either vanishes, or acts so strongly that it removes the event from the two-particle correlation. It has been suggested that such an effect may result from a surface bias, which selects predominantly back-to-back particle production tangential to the collision region [58].

Aside of Monte Carlo event generators, which are tailored to the simulation of multi-particle final states, there is also one recent analytical approach towards calculating triggered two-particle correlation functions and their medium dependence [59, 60].

We finally mention a third class of correlation measurements:

**Triggered away-side particle-jet (photon/ $Z$ -boson)-jet correlations.** Ideally, if one triggers on a prompt photon or  $Z$ -boson, one knows the energy of the recoil parton. For sufficiently high trigger  $p_T$ , the recoil will be a jet, whose medium-modification can be characterized above background by all the quantities discussed in section 2. Since photons and  $Z$ -bosons do not interact with the medium, one expects that the hard vertex at which the jet is produced, is distributed homogeneously over the transverse plane (no surface bias). Such measurements have been advocated [61] as an alternative to unbiased calorimetric jet determinations. In practice, one must understand to what extent the triggered photons are prompt. The need to reject efficiently photons from  $\pi^0$ -decays, and the need to accumulate sufficient yield limits such correlation measurements to the range of  $p_T^{\text{trig}} < 70$  GeV at the LHC [62, 63].  $Z$ -boson triggered jet samples are free from this difficulty but may be statistics limited. To bypass the constraints of limited statistics, there are also ideas that the fragmentation patterns of high- $p_T$  triggered hadrons may be understood sufficiently well to obtain useful characterizations of the recoil energy. We expect that such ideas will be scrutinized further in the coming years in a tight interplay between theory and experiment.

### 3.4 Features in the underlying event associated to high- $p_T$ triggers

By triggering on a high- $p_T$  particle or calorimetric tower, one selects events which differ from minimum bias also with respect to their soft particle distribution. Some, but not necessarily all of these differences may arise from the soft fragments of the high- $p_T$  final state partons. One may group conceivable effects into two classes:

**Medium-modifications of the parton fragmentation at large  $\xi$ , i.e. at low  $p_T$ .** Jet quenching implies an increase of soft particle multiplicity above background, which may be visible above background, see section 2.3.3. A number of medium effects have been suggested, which may leave characteristic imprints on this soft yield associated to high- $p_T$  triggers. For instance, medium-induced gluon radiation may result in the broadening of the soft multiplicity in a jet [64], and it may give rise to a double-peaked structure in two-particle correlations [65]. Also, the soft multiplicity in a jet may be distorted characteristically by a flow field [66], or it may receive additional contributions from target components, which are kicked by elastic recoil effects into the jet cone. Possibly the most characteristic modification would be the emergence of a Mach cone, resulting from the fact that the parton projectile loses energy by exciting sound modes in the medium [67, 68]. One common hallmark of all these effects is that the energy contained in the soft structure above background and the energy contained in the high- $p_T$  trigger must add up to the energy of the parent parton, which in principle can be constrained independently.

#### **Features in the underlying event not related to final state parton fragmentation.**

In a hadronic collision which contains a jet, not all the soft hadron multiplicity produced above background results from the fragmentation of the outgoing hard parent partons. It is known since long that requiring a high transverse momentum hadronic structure in the collision increases the multiplicity in the underlying event over a wide range in rapidity [69]. At least part of this so-called pedestal of the underlying event results from the fact that triggering on a high- $Q^2$  process implies additional initial state radiation, which is spread in rapidity.

For the study of heavy ion collisions, this effect may be interesting, since it suggests a way of adding in a controlled and localized way additional multiplicity and energy to an event in a region which is well-separated from the high- $p_T$  trigger. One may then be in a position to study how the medium interacts with this perturbation. For instance, if the pedestal is carried by a transverse flow field, then it could be moved predominantly in the azimuthal direction of the triggered hadron since this direction is selected predominantly by the surface bias. A hadronic scenario closely related to this picture has been discussed in Ref. [70]. The result would be a "ridge", that is, an enhancement of multiplicity in a small  $p_T^{\text{assoc}}$ -range but over a wide range of rapidity, which shows up only at the side of the high- $p_T$  trigger. There is some evidence for such a structure at RHIC. LHC may help to clarify the dynamical origin of such structures since with increasing  $\sqrt{s}$ , the hadronic activity in both the incoming and outgoing state is expected to increase significantly with the trigger  $p_T$  and may manifest itself in a wider range of  $p_T^{\text{assoc}}$ .

## 4 High-energy parton propagation in dense QCD matter

At high transverse energy the medium-modification of jets and of single inclusive hadron spectra and jet-like hadron correlations is dominated by modification of the partonic propagation prior to hadronization. This is supported by data from RHIC (see subsection 3.1) and by parametric estimates (see subsection 2.1). It motivates us in the present chapter to review aspects of the in-medium propagation of partons.

The interaction of an energetic projectile with a component of a medium can be classified according to whether it proceeds via elastic processes (multiple scattering without particle production) or via inelastic processes. In the phenomenology of heavy ion collisions, these processes are often referred to as radiative and collisional parton energy loss, respectively. In addition, virtual partons can split without interacting with the medium. In the following, we discuss these three components of in-medium parton propagation. We start by discussing the ultra-relativistic limit of very large projectile energy ( $E \rightarrow \infty$ ), where parton propagation can be described in the eikonal formalism.

### 4.1 Parton propagation through dense QCD matter in the eikonal formalism

In-medium parton propagation can be described by solving the Dirac equation for the wave function of a parton in the spatially extended color field of the target. In the limit of infinite projectile energy, the solution of this Dirac equation can be written in terms of the eikonal factor

$$W(\mathbf{x}_i) = \mathcal{P} \exp\left\{i \int dz^- T^a A_a^+(\mathbf{x}_i, z^-)\right\}. \quad (4.1)$$

Here,  $A^+$  is the large component of the target color field and  $T^a$  is the generator of  $SU(N)$  in the representation corresponding to a given parton. Here and in what follows, we use bold-face variables such as  $\mathbf{x}_i$  to denote 2-dimensional vectors which lie in the plane orthogonal to the beam direction. Equation (4.1) is the specific form of the phase factor in the light cone gauge  $A^- = 0$  for a projectile moving in the negative  $z$  direction, so that the light cone coordinate  $x^+ = (z + t)/\sqrt{2}$  does not change during propagation through the target. The phase factor takes a different form in other gauges or other Lorentz frames, but the final result is gauge invariant and Lorentz covariant, of course.

To be specific, let us consider a high-energy quark of color  $\alpha$  at transverse position  $\mathbf{x}$  with incoming wave function  $|\alpha(\mathbf{x})\rangle$ . Scattering on the target results in the outgoing wave function

$$\mathcal{S}|\alpha(\mathbf{x})\rangle = W(\mathbf{x})_{\beta\alpha}|\alpha(\mathbf{x})\rangle. \quad (4.2)$$

This wave function is the solution of the Dirac equation in the external color field  $A^+$  and in the limit of infinite projectile energy. More generally, the eikonal formalism describes the interaction of any set of projectile partons with the target by a color rotation  $\alpha_i \rightarrow \beta_i$  of each projectile component  $i$ , resulting in an eikonal phase  $W(\mathbf{x}_i)_{\alpha_i\beta_i}$ . The out-going wave function  $W(\mathbf{x})_{\beta\alpha}|\{\alpha, \mathbf{x}\}\rangle$ . Here, the physics is that

in the ultra-relativistic limit, the target is Lorentz contracted to an infinitesimally thin pancake in the rest frame of the projectile. As a consequence, the projectile cannot change its transverse position during the interaction, it propagates on an eikonal straight-line trajectory. In this limit, interactions with the target are recoilless (and hence, there is no collisional energy loss) and they lead to the color rotation of each projectile component according to (4.1). If different components acquire a different relative phase due to interactions with the target, then these components of the incoming hadron wave function decohere in the scattering. This decoherence is at the basis of many formulations of radiative energy loss, and hence we discuss it here explicitly in the simplest case within the eikonal formalism. For more details about the eikonal formalism, we refer to Ref. [71] and references therein.

**Example: gluon radiation off high-energy quark in the eikonal formalism.** We consider a high energy quark, which impinges on the target with a fully developed wave function. In the first order in perturbation theory the incoming wave function contains the Fock state  $|\alpha\rangle$  of the bare quark, supplemented by the coherent state of quasi real gluons which build up the Weizsäcker-Williams field  $f(\mathbf{x})$ ,

$$|\Psi_{\text{in}}^\alpha\rangle = |\alpha\rangle + \int d\mathbf{x} d\xi f(\mathbf{x}) T_{\alpha\beta}^b |\beta; b(\mathbf{x}, \xi)\rangle. \quad (4.3)$$

Here Lorentz and spin indices are suppressed. In the projectile light cone gauge  $A^- = 0$ , the gluon field of the projectile is the Weizsäcker-Williams field

$$A^i(\mathbf{x}) \propto \theta(x^-) f_i(\mathbf{x}), \quad f_i(\mathbf{x}) \propto g \frac{\mathbf{x}_i}{x^2}, \quad (4.4)$$

where  $x^- = 0$  is the light cone coordinate of the quark in the wave function. The integration over the rapidity of the gluon in the wave function (4.3) goes over the gluon rapidities smaller than that of the quark. In the leading logarithmic order the wave function does not depend on rapidity and we suppress the rapidity label in the following. The outgoing wave function reads

$$|\Psi_{\text{out}}^\alpha\rangle = W_{\alpha\gamma}^F(\mathbf{0}) |\gamma\rangle + \int d\mathbf{x} f(\mathbf{x}) T_{\alpha\beta}^b W_{\beta\gamma}^F(\mathbf{0}) W_{bc}^A(\mathbf{x}) |\gamma; c(\mathbf{x})\rangle, \quad (4.5)$$

where  $W^F(\mathbf{0})$  and  $W^A(\mathbf{x})$  are the Wilson lines in the fundamental and adjoint representations respectively, corresponding to the propagating quark at the transverse position  $\mathbf{x}_q = \mathbf{0}$  and gluon at  $\mathbf{x}_g = \mathbf{x}$ .

The projection of the outgoing wave function  $\Psi_{\text{out}}$  on the subspace spanned by incoming quark wave functions will describe outgoing quarks which are 'dressed' with gluons. Hence, to count the number of newly produced gluons in the state (4.5), one must select the projection of  $\Psi_{\text{out}}$  on the subspace orthogonal to the incoming states

$$|\delta\Psi_\alpha\rangle = |\Psi_{\text{out}}^\alpha\rangle - \sum_\gamma |\Psi_{\text{in}}(\gamma)\rangle \langle\Psi_{\text{in}}(\gamma)|\Psi_{\text{out}}^\alpha\rangle. \quad (4.6)$$

Here, the index  $\gamma$  in the projection operator runs over the quark color index, so that the second term in (4.6) projects out the entire Hilbert subspace of incoming states.

The number spectrum of produced gluons is obtained by calculating the number of gluons in the state  $\delta\Psi_\alpha$ , averaged over the incoming color index  $\alpha$ . After some color algebra, one obtains

$$\begin{aligned} N_{\text{prod}}(\mathbf{k}) &= \frac{1}{N} \sum_\alpha \langle \delta\Psi_\alpha | a_d^\dagger(\mathbf{k}) a_d(\mathbf{k}) | \delta\Psi_\alpha \rangle \\ &= \frac{\alpha_s C_F}{2\pi} \int d\mathbf{x} d\mathbf{y} e^{i\mathbf{k}\cdot(\mathbf{x}-\mathbf{y})} \frac{\mathbf{x}\cdot\mathbf{y}}{x^2 y^2} \left[ 1 - \frac{1}{N^2-1} \langle\langle \text{Tr} [W^{A\dagger}(\mathbf{x}) W^A(\mathbf{0})] \rangle\rangle_t \right. \\ &\quad \left. - \frac{1}{N^2-1} \langle\langle \text{Tr} [W^{A\dagger}(\mathbf{y}) W^A(\mathbf{0})] \rangle\rangle_t \right. \\ &\quad \left. + \frac{1}{N^2-1} \langle\langle \text{Tr} [W^{A\dagger}(\mathbf{y}) W^A(\mathbf{x})] \rangle\rangle_t \right]. \quad (4.7) \end{aligned}$$

Here, we have used  $f(\mathbf{x})f(\mathbf{y}) = \frac{\alpha_s}{2\pi} \frac{\mathbf{x}\cdot\mathbf{y}}{\mathbf{x}^2\mathbf{y}^2}$  for the Weizsäcker-Williams field of the quark projectile in configuration space and the symbol  $\langle\langle \dots \rangle\rangle_t$  denotes the averaging over the gluon fields of the target.

We emphasize three findings, which are seen explicitly in the eikonal formalism presented here, and which persist in a more general treatment:

- *Radiative energy loss dominates over collisional energy loss at high energy.*

At high projectile energy, momentum transfer between projectile and target is predominantly transverse. Longitudinal momentum transfer is suppressed by powers of projectile energy. Hence, in the eikonal formalism the projectile does not transfer longitudinal momentum to target components via elastic interactions. In contrast, the eikonal formalism allows for the calculation of inelastic processes, as discussed above. This illustrates that radiative mechanisms are the dominant source of medium modification for sufficiently high parton energy.

- *A light-like Wilson loop defines the medium-dependence of the gluon spectrum.*

As seen from the radiation spectrum (4.7), the entire information about the target resides in the target average of two light-like adjoint Wilson lines. Although the presence of quarks leads to the appearance of fundamental Wilson lines in intermediate stages of the calculation, see e.g. equation (4.5), the averaging involved in (4.7) combines them into adjoint ones with the help of the Fierz identity  $W_{ab}^F(\mathbf{x}) = 2 \text{Tr} [T^a W^{F\dagger}(\mathbf{x})T^b W^F(\mathbf{x})]$ .

- *Particle production in the eikonal formalism is determined by a decoherence effect.*

The above calculation provides an explicit example for the general statement, that gluons are emitted from a parton projectile if and only if they have accumulated due to medium interactions a relative phase of order unity with respect to other partonic projectile components.

## 4.2 Gluon radiation off quarks produced in the medium

In section 4.1, we considered radiation off a quark, which propagated a long distance before impinging on the target. This quark had a fully evolved wave function, that means, it had time to develop a gluon cloud around it. Medium-induced radiation amounts to the partial stripping of these quasi real gluons in the quark wavefunction. In the present section, we discuss medium-induced gluon radiation off a parton, which is produced in a large momentum transfer process *inside the medium*. This problem is significantly more complicated mainly because of two issues:

- *Interference between radiation in the vacuum and medium-induced radiation*

In the absence of a medium, a parton produced in a hard process will radiate its large virtuality  $Q$  on a typical timescale  $1/Q$  by developing a parton shower. In the rest frame of the medium, this time scale is Lorentz dilated by a factor  $E_{\text{parton}}/M$ , where the parton mass is  $M \sim Q$ . Typical radiation times  $\sim E_{\text{parton}}/Q^2$  are comparable to the typical in-medium pathlengths in a nucleus-nucleus collision. As a consequence, one expects an interference pattern between the radiation present in the vacuum, and the additional radiation induced due to scattering in the medium.

- *Corrections to eikonal approximation*

In the ultra-high energy (eikonal) approximation, the longitudinal extension of the target is contracted to a delta function. As a consequence, gluon radiation off a hard parton occurs either before or after the target, but not within the target. In contrast, to take interference effects into account, it is important to locate the gluon emission vertex inside the medium. This requires a formulation which is sensitive to longitudinal distances (or the time spent) in the medium. The momentum conjugate to this distance is the projectile energy  $E$  or light cone energy  $p_-$ . So, to place an emission vertex within the medium, one has to keep track at least of the  $O(1/p_-)$ -corrections to the eikonal formalism.

### 4.2.1 Gluon radiation in the path integral formalism

In the following, we present the main elements of a formulation which goes beyond the eikonal approximation and accounts for interference effects between vacuum and medium-induced radiation. Up to order



$O(1/p^-)$ , one can write the solution  $\Psi_{\text{out}}(\mathbf{r}_{\text{out}}, x_{\text{out}}^-) = \int d\mathbf{r}_{\text{in}} G(\mathbf{r}_{\text{in}}, x_{\text{in}}^-; \mathbf{r}_{\text{out}}, x_{\text{out}}^- | p^-) \Psi_{\text{out}}(\mathbf{r}_{\text{in}}, x_{\text{in}}^-)$  of the Dirac equation for a colored partonic projectile propagating in a spatially extended color field  $A^+$  in terms of the light-cone Green's function [72–75]

$$G(\mathbf{r}_{\text{in}}, x_{\text{in}}^-; \mathbf{r}_{\text{out}}, x_{\text{out}}^- | p^-) = \int_{\mathbf{r}(x_{\text{in}}^-)=\mathbf{r}_{\text{in}}}^{\mathbf{r}(x_{\text{out}}^-)=\mathbf{r}_{\text{out}}} \mathcal{D}\mathbf{r}(\xi) \exp \left[ i \frac{p^-}{4} \int_{x_{\text{in}}^-}^{x_{\text{out}}^-} d\xi \dot{\mathbf{r}}^2(\xi) \right] W(\mathbf{r}(\xi); x_{\text{in}}^-, x_{\text{out}}^-), \quad (4.8)$$

$$W(\mathbf{r}; x_{\text{in}}^-, x_{\text{out}}^-) = \mathcal{P} \exp \left[ i \int_{x_{\text{in}}^-}^{x_{\text{out}}^-} d\xi A^+(\mathbf{r}(\xi), \xi) \right]. \quad (4.9)$$

This solution contains a non-eikonal Wilson line, which 'wiggles' in transverse position along a path  $\mathbf{r}(\xi)$ . In the limit of ultra-high parton energy,  $p^- \rightarrow \infty$ , when the finite energy corrections of order  $O(1/p^-)$  vanish, this expression reduces to the eikonal Wilson line (4.1),

$$\lim_{p^- \rightarrow \infty} G(\mathbf{r}_{\text{in}}, x_{\text{in}}^-; \mathbf{r}_{\text{out}}, x_{\text{out}}^- | p^-) = W(\mathbf{r}_{\text{in}}; x_{\text{in}}^-, x_{\text{out}}^-) \delta^{(2)}(\mathbf{r}_{\text{out}} - \mathbf{r}_{\text{in}}). \quad (4.10)$$

In the eikonal formalism, gluon radiation (4.7) is determined by the target average of two eikonal Wilson lines  $\langle \langle \text{Tr} [W^{A^\dagger}(\mathbf{y}) W^A(\mathbf{0})] \rangle \rangle_t$ . In close analogy, it is the target average of pairs of Green's functions  $\mathcal{K}$ , which determines gluon radiation in the present formalism. This target average can be defined in terms of the two-point correlation function of the target color field, see Ref. [3, 76] for technical details. If this color field is parametrized by a set of static scattering centers of path-dependent density  $n(\xi)$ , then the target average can be written as [73, 77]

$$\mathcal{K}(\mathbf{r}', z'; \mathbf{r}, z | \mu) = \int \mathcal{D}\mathbf{r} \exp \left[ i \int_z^{z'} d\xi \left[ \frac{\mu}{2} \dot{\mathbf{r}}^2 + i \frac{1}{2} n(\xi) \sigma(\mathbf{r}) \right] \right]. \quad (4.11)$$

Here,  $\sigma(\mathbf{r})$  is the so-called dipole cross section, which is defined in terms of the Fourier transform of the elastic cross section between scattering center and target. One novel feature of the target average of two Green's functions (4.8) is that the average depends on the energies  $\alpha p$  and  $(1 - \alpha)p$  in the arguments of both Green's functions. For this reason,  $\mathcal{K}$  in (4.11) depends on  $\mu \equiv \alpha(1 - \alpha)p$ . In accordance with the notation used in parton energy loss calculations, we have changed from light-cone coordinates to the longitudinal  $z$ . One can check that the  $\mu \rightarrow \infty$  limit of (4.11) leads to the average of two eikonal Wilson lines, entering (4.6).

The inclusive energy distribution of gluon radiation off an in-medium produced parton can be expressed in terms of the path integral (4.11) as [77]

$$\omega \frac{dI}{d\omega} = \frac{\alpha_s C_R}{(2\pi)^2 \omega^2} 2\text{Re} \int_{\xi_0}^{\infty} dy_l \int_{\bar{y}_l}^{\infty} d\bar{y}_l \int d\mathbf{u} \int_0^{\chi\omega} d\mathbf{k} e^{-i\mathbf{k}\cdot\mathbf{u}} e^{-\frac{1}{2} \int_{\bar{y}_l}^{\infty} d\xi n(\xi) \sigma(\mathbf{u})}$$

$$\times \frac{\partial}{\partial \mathbf{y}} \cdot \frac{\partial}{\partial \mathbf{u}} \int_{\mathbf{y}=0}^{\mathbf{u}=\mathbf{r}(\bar{y}_l)} \mathcal{D}\mathbf{r} \exp \left[ i \int_{y_l}^{\bar{y}_l} d\xi \frac{\omega}{2} \left( \dot{\mathbf{r}}^2 - \frac{n(\xi) \sigma(\mathbf{r})}{i\omega} \right) \right]. \quad (4.12)$$

Here,  $\mathbf{k}$  denotes the transverse momentum of the emitted gluon. The two-dimensional transverse coordinates  $\mathbf{u}$ ,  $\mathbf{y}$  and  $\mathbf{r}$  emerge in the derivation of (4.12) as distances between the positions of projectile components in the amplitude and complex conjugate amplitude. The longitudinal coordinates  $y_l$ ,  $\bar{y}_l$  integrate over the ordered longitudinal gluon emission points in amplitude and complex conjugate amplitude. The limit  $|\mathbf{k}| < \chi\omega$  on the transverse phase space restricts gluon emission to a finite opening angle  $\Theta$ ,  $\chi = \sin \Theta$ . For the full angular integrated quantity,  $\chi = 1$ .

There are two limiting cases, in which the compact expression (4.12) for the medium-induced gluon energy distribution can be related to several currently used formalism of parton energy loss:

**Opacity expansion:** [77, 78] An expansion in powers of opacity is obtained by expanding the integrand of (4.12) in powers of the dipole cross section  $\sigma(\mathbf{r})$ . In so-called Gyulassy-Wang models [79], where the color field strength of the medium is parametrized in terms of a set of static scattering centers of density  $n(\xi)$ ,

$$\sigma(\mathbf{r}) = 2 \int \frac{d\mathbf{q}}{(2\pi)^2} |A(\mathbf{q})|^2 (1 - \exp\{i \mathbf{q} \cdot \mathbf{r}\}) . \quad (4.13)$$

Here,  $A(\mathbf{q})$  is the potential of a single scattering center (for more details, including the treatment of color in potential scattering, see Ref. [3]).

In the absence of a medium, that is, to zeroth order in opacity, one finds

$$\omega \frac{d^3 I(N=0)}{d\omega d\mathbf{k}} = \frac{\alpha_s}{\pi^2} C_R \frac{1}{\mathbf{k}^2}, \quad H(\mathbf{k}) = \frac{1}{\mathbf{k}^2}. \quad (4.14)$$

This is the characteristic  $1/\mathbf{k}^2$ -gluon radiation spectrum associated to the DGLAP parton branching process in the vacuum. Expression (4.14) illustrates that the gluon energy distribution (4.12) contains information about the off-shellness of the projectile parton, since it allows for gluon radiation without medium interaction.

For a medium of constant density  $n(\xi) = n_0$  and longitudinal extension  $L$ , the contribution to (4.12) to first order of opacity takes the form

$$\omega \frac{d^3 I(N=1)}{d\omega d\mathbf{k}} = \frac{\alpha_s}{\pi^2} \frac{C_R}{2\omega^2} \int \frac{d\mathbf{q}_1}{(2\pi)^2} |a_0(\mathbf{q}_1)|^2 (\mathbf{k} \cdot \mathbf{q}_1) n_0 \tau \tau_1^2 \left[ \frac{L}{\tau_1} - \sin\left(\frac{L}{\tau_1}\right) \right], \quad (4.15)$$

where

$$\tau = \frac{2\omega}{\mathbf{k}^2}, \quad \tau_1 = \frac{2\omega}{(\mathbf{k} - \mathbf{q}_1)^2}. \quad (4.16)$$

This is an explicit illustration of the formation time physics discussed in section 2.1. The interference term  $\left[ \frac{L}{\tau_1} - \sin\left(\frac{L}{\tau_1}\right) \right]$  in (4.15) prevents gluons from being radiated if  $L < \tau_1$ . According to the discussion of equation (2.5),  $\tau_1$  can be regarded as the formation time of the emitted gluon prior to interaction with target. The condition  $L/\tau_1 < 1$  then translates into the simple statement that a gluon can only scatter if at the time of the scattering it is an independent component of projectile wave function, that means, if it is formed. The generalization of this observation can be used for a probabilistic implementation of medium-induced interference effects, see section 4.4.3

In general, the medium-induced gluon energy distribution (4.12) receives contributions from vacuum radiation, from the elastic scattering of vacuum radiation on the medium, and from additional medium-induced radiation. These three contributions can be clearly isolated in the formal limit of a large distance between the location of projectile production and interaction with the medium. This can be done in the incoherent limit in which  $L \rightarrow \infty$  but  $n_0 L = \text{fixed}$ . Up to first order in opacity, one finds

$$\lim_{L \rightarrow \infty} \sum_{m=0}^{N=1} \omega \frac{d^3 I(m)}{d\omega d\mathbf{k}} = \frac{\alpha_s}{\pi^2} C_F (1 - w_1) H(\mathbf{k}) + \frac{\alpha_s}{\pi^2} C_F n_0 L \int \frac{d\mathbf{q}_1}{(2\pi)^2} |a_0(\mathbf{q}_1)|^2 \left( H(\mathbf{k} + \mathbf{q}_1) + R(\mathbf{k}, \mathbf{q}_1) \right). \quad (4.17)$$

Here,  $H(\mathbf{k})$  is the hard, medium-independent radiation (4.14) reduced by the probability  $w_1$  that one interaction of the projectile occurs in the medium. The second term describes the hard radiation component which rescatters once in the medium. The third term is the medium-induced Gunion-Bertsch contribution  $R(\mathbf{k}, \mathbf{q}_1)$  for additional gluon radiation. For realistic kinematical conditions, interference terms as e.g. in (4.16) interpolate between these simple and physically intuitive limiting cases.

It has been pointed out that the opacity expansion may have bad convergence properties [80]. On the other hand, comparisons of numerical results for the  $N = 1$  opacity expansion and the multiple soft scattering approximation discussed below show that both approaches can be brought to quantitative agreement on key parameters.

**Multiple soft scattering approximation** [73, 74, 77, 81–83] The medium-induced gluon energy distribution (4.12) can be studied in the saddle point approximation, where it is sensitive to the short distance behavior of the dipole cross section

$$n(\xi) \sigma(\mathbf{r}) \simeq \frac{1}{2} \hat{q}(\xi) \mathbf{r}^2. \quad (4.18)$$

Here,  $\hat{q}(\xi)$  is referred to as BDMPS (Baier-Dokshitzer-Mueller-Peigné-Schiff) transport coefficient. The path integral becomes that of a harmonic oscillator and can be calculated explicitly. Typical numerical results for the medium-induced gluon energy distribution (4.12) are shown in Figure 5 for a static BDMPS transport coefficient  $\hat{q} = \hat{q}(\xi)$  extending over a finite in-medium pathlength  $L$ . As explored first in [84],

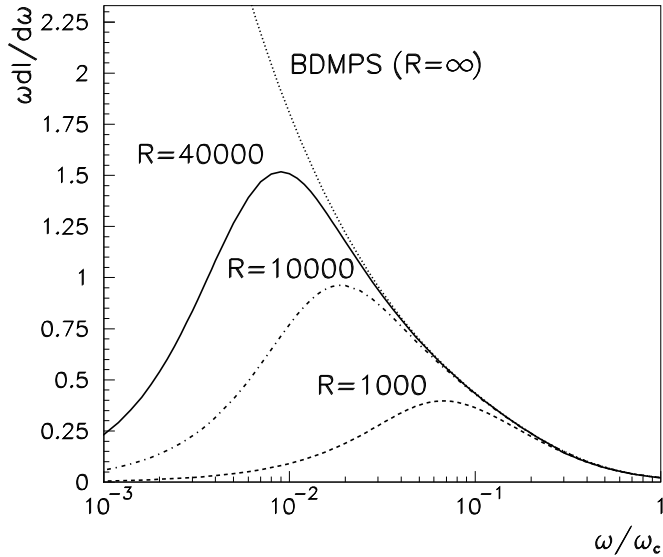


Figure 5: The medium-induced gluon energy distribution  $\omega \frac{dI}{d\omega}$  as a function of the gluon energy  $\omega$  in units of  $\omega_c = \frac{1}{2} \hat{q} L^2$ , and for different values of the kinematic constraint  $R = \omega_c L$ . Figure taken from Ref. [86].

the path integral (4.12) allows for a saddle point approximation also for the case of time-dependent densities and quenching parameters of the form

$$\hat{q}(\xi) = \hat{q}_d \left( \frac{\xi_0}{\xi} \right)^\alpha. \quad (4.19)$$

Here,  $\hat{q}_d$  is the value of  $\hat{q}$ , taken at the initial plasma formation time  $\xi_0$ . The power  $\alpha = 0$  characterizes the static medium discussed above. The value  $\alpha = 1$  is obtained for a system with one-dimensional, boost-invariant longitudinal expansion. In general, one can encode with a suitable choice of  $\alpha$  for the characteristic density decrease resulting from the expansion of the collision region. Remarkably, the radiation spectrum  $\omega \frac{dI}{d\omega}$  satisfies a simple scaling law which relates the radiation spectrum of a dynamically expanding collision region to an equivalent static scenario. The linearly weighed line integral [85]

$$\bar{\hat{q}} = \frac{2}{L^2} \int_{\xi_0}^{\xi_0+L} d\xi (\xi - \xi_0) \hat{q}(\xi) \quad (4.20)$$

defines the transport coefficient of the equivalent static scenario. The gluon energy distribution (4.12) of an expanding scenario (4.19) is approximately equal to the gluon energy distribution of a static scenario with  $\hat{q}(\xi) = \bar{q}$ . The linear weight in (4.32) implies that scattering centers which are further separated from the production point of the hard parton are more effective in leading to partonic energy loss.

#### 4.2.2 Qualitative features of medium-induced gluon radiation

Main features of the gluon energy distribution in Fig. 5 can be understood in terms of qualitative arguments. We consider a gluon in the hard parton wave function. This gluon is emitted due to multiple scattering if it picks up sufficient transverse momentum to decohere from the partonic projectile. For this, the average phase  $\varphi$  accumulated by the gluon should be of order one or larger,

$$\varphi = \left\langle \frac{k_{\perp}^2}{2\omega} \Delta z \right\rangle \sim \frac{\hat{q} L}{2\omega} L = \frac{\omega_c}{\omega}. \quad (4.21)$$

Thus, from a hard parton traversing a finite path length  $L$  in the medium, gluons will be emitted up to a ‘‘characteristic gluon frequency’’

$$\omega_c = \frac{1}{2} \hat{q} L^2. \quad (4.22)$$

For an estimate of the shape of the energy distribution, we consider the number  $N_{\text{coh}}$  of scattering centers which add coherently in the gluon phase (4.21),  $k_T^2 \simeq N_{\text{coh}} \langle q_T^2 \rangle_{\text{med}}$ . Based on expressions for the coherence time of the emitted gluon,  $t_{\text{coh}} \simeq \frac{\omega}{k_T^2} \simeq \sqrt{\frac{\omega}{\hat{q}}}$  and  $N_{\text{coh}} = \frac{t_{\text{coh}}}{\lambda} = \sqrt{\frac{\omega}{\langle q_T^2 \rangle_{\text{med}} \lambda}}$ , one estimates for the gluon energy spectrum per unit path length

$$\omega \frac{dI}{d\omega dz} \simeq \frac{1}{N_{\text{coh}}} \omega \frac{dI^{\text{scatt}}}{d\omega dz} \simeq \frac{\alpha_s}{t_{\text{coh}}} \simeq \alpha_s \sqrt{\frac{\hat{q}}{\omega}}. \quad (4.23)$$

This  $1/\sqrt{\omega}$ -energy dependence of the medium-induced non-abelian gluon energy spectrum is expected for sufficiently small  $\omega < \omega_c$ . This dependence is seen in Fig. 5 to be realized by the full expression (4.12), if one neglects (as for the above estimate) kinematical constraint in transverse phase space, which cut-off the energy distribution in the infrared. For the  $\omega$ -integrated average parton energy loss, one finds from the above pocket estimates by integrating the differential distribution (4.23) over the in-medium path length  $L$  and over the gluon energy  $\omega$  up to  $\omega_c$ ,

$$\langle \Delta E \rangle = \int_0^{\omega_c} d\omega \omega \frac{dI}{d\omega} = \frac{\alpha_s C_R}{2} \omega_c \propto \hat{q} L^2. \quad (4.24)$$

The same parametric dependence  $\propto \hat{q} L^2$  can be found  $R = \omega_c L \rightarrow \infty$  at  $\omega_c = \text{fixed}$  [86]. This is the famous BDMPS-result that the average radiative energy loss grows quadratically with in-medium path length for sufficiently small  $L$ . The pocket estimate (4.23) encodes the main features of the BDMPS result, namely the correct small- $\omega$  behavior as well as the correct dependence of the average energy loss on density and in-medium path length.

We finally summarize the main results following from the medium-induced gluon energy distribution (4.12):

- The average parton energy loss grows parametrically like

$$\Delta E \propto L^2. \quad (4.25)$$

- The gluon radiation shows a characteristic hierarchical dependence on the color charge and mass of the parton projectile

$$\Delta E_{\text{gluon}} > \Delta E_{\text{lightquark}} > \Delta E_{\text{heavyquark}}. \quad (4.26)$$

Here, the first inequality follows from the larger color charge of partons in the adjoint representation. The second inequality is due to the dead cone effect, which suppresses radiation off massive particles in the vacuum and in the medium [87–90]. Several studies have analyzed the extent to which the hierarchy (4.26) affects the suppression patterns of heavy-flavored single inclusive hadron spectra and single electron spectra, which are dominated at sufficiently high transverse momentum by the semi-leptonic decays of heavy-flavored hadrons. [91, 92]. For a concise mini-review of approaches with focus on lower transverse momentum, see Ref. [93].

- The average transverse momentum of medium-induced gluon radiation grows as expected for Brownian motion resulting from multiple scattering,

$$\langle k_T^2 \rangle \propto \hat{q} L. \quad (4.27)$$

- The formalism studied in this section is recoilless. It neglects contributions to parton energy loss, that result from longitudinal momentum transfer to target degrees of freedom. To improve on this point, one requires a dynamical description of target degrees of freedom.
- The  $\omega$ -dependence of the gluon energy distribution shows a characteristic steepening due to medium-effects, see e.g. the  $\sqrt{\omega}$ -modification of (4.23).

### 4.2.3 Multiple gluon emission

The formalism discussed in this section 4.2 is based on calculating matrix elements for one-gluon emission. To describe the energy degradation of a highly energetic parton in dense QCD matter, one needs to account for the possibility that a total energy  $\Delta E$  is carried away by the emission of an arbitrary number of  $n$  gluons. In the absence of information about the medium-dependence of  $n$ -gluon emission cross sections, it has been proposed [47] to treat subsequent gluon emissions as independent. The probability distribution  $P(\Delta E)$  of losing a total energy  $\Delta E$  in the emission of an arbitrary number of gluons is then

$$P(\Delta E) = \sum_{n=0}^{\infty} \frac{1}{n!} \left[ \prod_{i=1}^n \int d\omega_i \frac{dI(\omega_i)}{d\omega} \right] \delta \left( \Delta E - \sum_{i=1}^n \omega_i \right) e^{-\int d\omega \frac{dI}{d\omega}}. \quad (4.28)$$

These probabilities are referred to as quenching weights. In general, they have a discrete and a continuous part, [85]

$$P(\Delta E) = p_0 \delta(\Delta E) + p(\Delta E). \quad (4.29)$$

The discrete weight  $p_0 = e^{-\int d\omega \frac{dI}{d\omega}}$  is a consequence of a finite mean free path. It denotes the probability that no additional gluon is emitted due to in-medium scattering and hence no medium-induced energy loss occurs. Quenching weights have been calculated for several formalism of radiative parton energy loss.

If one treats the medium-induced gluon energy distribution  $\omega \frac{dI}{d\omega}$  explicitly as the medium modification of a “vacuum” distribution [86]

$$\omega \frac{dI^{(\text{tot})}}{d\omega} = \omega \frac{dI^{(\text{vac})}}{d\omega} + \omega \frac{dI}{d\omega}, \quad (4.30)$$

one can write the total probability of losing parton energy via vacuum or medium-induced radiation as the convolution of (4.28) with the probability of vacuum energy loss

$$P^{(\text{tot})}(\Delta E) = \int_0^{\infty} d\bar{E} P(\Delta E - \bar{E}) P^{(\text{vac})}(\bar{E}). \quad (4.31)$$

Since gluon radiation in the vacuum underlies the scale dependence of fragmentation functions, this motivates models of medium-modified fragmentation functions, in which the vacuum fragmentation function

is convoluted with (4.28). More specifically, if the parent parton loses with probability  $P(\epsilon)$  an additional energy fraction  $\epsilon = \frac{\Delta E}{E_q}$  prior to hadronization, then the leading hadron is a fragment of a parton with lower energy  $(1 - \epsilon)E_q$ ; thus, it carries a larger fraction  $\frac{x}{1-\epsilon}$  of the initial parton energy. The inclusion of this effect amounts to replacing the fragmentation function  $D_{f \rightarrow h}(x, Q^2)$  in (2.1) by the medium-modified fragmentation function [61, 94]

$$D_{f \rightarrow h}^{(\text{med})}(x, Q^2) = \int_0^1 d\epsilon P(\epsilon) \frac{1}{1-\epsilon} D_{f \rightarrow h}\left(\frac{x}{1-\epsilon}, Q^2\right). \quad (4.32)$$

For alternative approaches towards medium-modified fragmentation functions, see Refs. [95–98].

#### 4.2.4 BDMPS, Z, ASW, GLV, ... and all that

A significant part of the literature on medium-induced gluon radiation can be related to limiting cases of the gluon energy distribution (4.12):

- **BDMPS** [47, 82, 83] is obtained from (4.12) in the multiple soft scattering approximation (4.18), using the limit

$$\omega \frac{dI^{(\text{BDMPS})}}{d\omega}(\omega_c \equiv \hat{q}L^2/2) = \lim_{R=\omega_c L \rightarrow \infty} \omega \frac{dI^{(\text{BDMPS})}}{d\omega}(\omega_c = \text{fixed}). \quad (4.33)$$

- **Zakharov** [73–75] has derived the BDMPS-result independently by a very different approach. In particular, he was the first to introduce the path-integral, with which equation (4.12) can be written in a compact form. It would be historically correct to refer to this formalism as BDMPS-Z.
- **ASW** [77, 81, 86, 88] The specific form (4.12) goes beyond 4.33 in that it is valid for arbitrary values of  $R = \omega_c L$ . In this way, it includes effects from finite in-medium path length  $L$  (which result e.g. in the infra-red cut-off of medium-induced gluon radiation seen in Figure 5) and it accounts for the rescattering effects in the  $k_T$ -differential gluon emission. This form was derived first in [77] and analyzed for massless [86] and massive [88]. partons subsequently. It has been analyzed in the multiple soft scattering approximation (4.18) and in the  $N = 1$  opacity expansion.
- **GLV** [78, 94] While ASW compares  $N = 1$  opacity expansion and multiple soft scattering limit, GLV focusses entirely on the opacity expansion of medium-induced gluon radiation, which had been studied first in [77] and in [78]. To first order in opacity, ASW and GLV obtain the same differential radiation cross sections.

We note that all above-mentioned formulations have been derived within the same kinematic region

$$E \gg \omega \gg |\mathbf{k}|, |\mathbf{q}| \equiv \left| \sum_i \mathbf{q}_i \right| \gg \Lambda_{\text{QCD}}. \quad (4.34)$$

That means, the energy  $E$  of the initial hard parton is much larger than the energy of the emitted gluon, which is much larger than its transverse momentum  $\mathbf{k}$  and the transverse momentum  $\mathbf{q}$  accumulated due to many scatterings of the projectile. By employing the above-mentioned formulations for phenomenological modeling, one inevitably extends their use beyond the range of their parametric validity (4.34). In particular, to calculate a  $k_T$ -integrated gluon energy distribution, one integrates the transverse momentum over the entire kinematical range  $|\mathbf{k}| \in [0, O(\omega)]$ . Moreover, to account for large parton energy loss, one allows for the case  $\omega \sim O(E)$ . Since exact energy-momentum conservation at the vertex is lost with the approximations (4.34), numerical results of these integrals depend inevitably on the cut-off procedures. For instance, the only difference between GLV and ASW lies in the implementation of these cut-offs outside the region (4.34). For the scope of the present review, we do not discuss these (important) details, which are at the basis of an ongoing debate, and which are currently evaluated quantitatively by the TECHQM Collaboration [55]. In the view of the present author, the best way to overcome the

phenomenological limitations resulting from the approximation (4.34) is to get rid of this approximation in the formulation of the medium-induced gluon radiation. While this is a very challenging task in analytical formulations, it can be achieved easily in Monte Carlo formulations, which we discuss in section 4.5.

We note that there are at least two other formulations of medium-induced gluon radiation, which are currently used in phenomenological modeling of parton energy loss

- **Higher-twist formalism** [95, 99, 100] This is a calculation of medium-induced gluon radiation, which describes properties of the medium in terms of 4-point "higher-twist" matrix elements. As for the formalisms discussed above, it can describe the interference between vacuum radiation and gluon radiation, which is phenomenologically important. This formalism shares many features with the above formalisms.
- **AMY** [101] While all approaches discussed above involve modeling in describing the interaction between projectile and target, this one does not. It is the only dynamically consistent, model-independent formulation of medium-induced gluon radiation, based solely on perturbative QCD. The price to pay for this theoretical clean situation is the limitation to a peculiar kinematic region in which projectile energies are of the order of the temperature, and where the temperature is very high ( $T \gg T_c$ ) so that hard-thermal-loop improved perturbation theory is applicable. Moreover, one neglects interference effects between vacuum and medium-induced gluon radiation, which are known from other studies to affect numerical results by large numbers. As a consequence, for phenomenological applications one must extrapolate this formalism significantly outside its strict range of validity.

### 4.3 Elastic interactions between projectile and medium

Collisional mechanisms of parton energy loss, mediated via elastic interactions, have been explored first in [102–104]. It was then observed that at sufficiently high projectile energy, an essentially recoilless radiative energy loss mechanism is expected to dominate on general kinematic grounds [74, 77, 78, 83, 99]. At sufficiently small projectile energies, however, recoil is expected to be non-negligible. Several recent model studies [54, 105–108] attribute a sizable role to collisional mechanisms mediated via elastic interactions.

Elastic interactions between a partonic projectile  $Q$  and degrees of freedom in the target can transfer per unit path length a fraction  $\Delta p_Q$  of the projectile momentum to the target. Multiple interactions add incoherently for elastic processes, so that

$$\frac{d\Delta p_Q}{dx} = \frac{1}{v_Q} \int dp_f (p - p_f) \int k^2 dk \left( n_q(k) \frac{d\sigma_{Qq}^{\text{int}}(k, p_f)}{dp_f} + \frac{9}{4} n_g(k) \frac{d\sigma_{Qg}^{\text{int}}(k, p_f)}{dp_f} \right). \quad (4.35)$$

Here,  $p$  is the initial and  $p_f$  the final momentum of the projectile  $Q$ , and  $v_Q$  denotes its velocity in the rest frame of the medium. By  $n_q(k)$  and  $n_g(k)$ , we denote the distribution of quark and gluon scattering centers of momentum  $k$  in the medium. The elastic scattering cross section can be written in the form

$$\frac{d\sigma^{\text{int}}}{dp_f} = 2\pi \int d(\cos \psi) \frac{1}{4p^0 k^0} |\mathcal{M}|^2 d\Phi, \quad (4.36)$$

where  $2\pi \int d(\cos \psi)$  denotes the integration over the direction of the incoming target particle, and  $d\Phi$  denotes the phase space volume.

Within this framework, models for collisional energy loss calculations are fully specified in terms of the densities  $n_q$ ,  $n_g$  and the elastic scattering matrix element  $\mathcal{M}$ . For the latter, one often uses the expression to lowest order in  $\alpha_s$  with single gluon exchange in the t-channel described by the HTL-resummed propagator. This is the starting point of many works on collisional energy loss, including the

early works! [103, 104]. There is a significant number of recent works, which implement variations of this formalism, such as not including any assumption about the smallness of momentum transfers [105], calculating for constant coupling constant [54, 105] or running coupling constant [109]. Also, there are different models, which parametrize the medium e.g. either as a set of massless particles with thermal momentum distribution [54, 105], or as a set of initially static massive scattering centers [108]. By making the target scattering centers dynamical, these models parametrize not only the color field strength but also the capacity of the medium to absorb recoil.

We limit our discussion to some generic observations:

- Elastic scattering cross sections are dominated by small-angle scattering involving small momentum transfer. As a consequence, the average collisional parton energy loss can be much larger than the typical parton energy loss encountered by a high- $p_T$ -triggered particle, as discussed in the section 3.1.
- Some recent models result in an average collisional parton energy loss which remains numerically significant over a wide transverse momentum range [54, 105, 109]. Although the size of this effect can depend significantly on the modeling of the medium, this indicates that collisional effects must not be neglected in the description of jet quenching.
- While the mass-ordering (4.26) of radiative energy loss depends on the projectile mass only, the mass-ordering of collisional energy loss is sensitive to the recoil properties of the medium and can be inverted compared to that of radiative energy loss [110].

#### 4.4 Monte Carlo Formulations of parton propagation in the medium

In the absence of a medium, the final state parton showers, encoded in modern Monte Carlo (MC) event generators [22–24], can account reliably for jet event shapes, jet substructures and the main features of other intra-jet characteristics, discussed in section 2.3. To discuss jet quenching on the level of multi-particle final states, it is of obvious interest to extend the applicability of MC final state parton showers to medium effects. Any such attempt must address two central issues:

- *Specifying the spatio-temporal embedding of jets in matter.*  
 In the absence of a medium, the length and time scales, over which branching processes occur, do not enter the evolution. Hence, the final state parton shower is formulated completely in momentum space. This is different in the presence of a medium, when length scales and time scales determine which branching processes occur inside the medium and how frequently the medium can interact with the parton shower. One may distinguish two aspects:
  - i) *Specifying the spatio-temporal evolution of the probe* amounts to a somewhat model-dependent choice, since it is difficult to constrain phenomenologically. This choice should be made consistent with what is known parametrically about the localization of partonic processes. In particular, a complete spatio-temporal ordering can be specified by attributing to each virtual parton in the branching process a lifetime of order  $\tau_{\text{virtual life}} = E/Q^2$  according to equation (2.4). Once data for in-medium modified jets are compared to MC simulations, this picture of the spatio-temporal embedding of jets in matter can be scrutinized in an interplay between experiment and MC modeling.
  - ii) *The spatio-temporal extension and evolution of the medium* is important, since parton energy loss can depend strongly on in-medium path length. The current state of the art of modeling high- $p_T$  hadron suppression uses information from hydrodynamical simulations of heavy ion collisions, or simple parametrizations thereof. There is also a class of model studies, which specifies the geometrical distribution of matter from the nuclear overlap of Glauber theory [49, 51].
- *Specifying the interactions between projectile and medium*  
 Simulations of the medium-modification of jets fragmentation can depend e.g. on the strength and kinematics of interactions between partonic projectiles and the medium, on the relative weight of elastic and inelastic processes, and on the probability with which these interactions occur per



unit path length. In general, varying the nature of these interactions amounts to varying properties of the medium. Hence, the model-dependence which comes with this broad array of conceivable interactions, is wanted. The extent to which the medium modification of jet fragmentation depends on assumptions about the interaction between projectile and medium determines the discriminatory power of jet quenching as a tool for characterizing properties of the medium. However, for the case of multiple interactions, the so-called non-abelian Landau-Pomeranchuk-Migdal effect, that is the destructive quantum interference between subsequent inelastic production processes, is known to strongly affect medium-induced radiative energy loss. Quantitative control of this interference is a prerequisite for determining the nature of interactions between projectile and medium.

In the following, we review shortly the current state of the art in encoding elastic and inelastic interactions with the medium in MC parton shower simulations. We focus mainly on formulations, which aim at implementing what is known analytically about in-medium parton propagation, as discussed in sections 4.2 and 4.3. For a self-contained presentation, we start with some remarks about final state parton showers in the vacuum. In what follows, we do not discuss further several Monte Carlo studies, which seem to account for the high- $p_T$  suppression patterns at RHIC by invoking specific implementations of non-perturbative physics, see e.g. [111–113].

#### 4.4.1 Parton shower in the vacuum

The MC algorithms for leading order final state parton showers in elementary collisions are documented in great detail in the literature [22–24]. There are different variants, which differ e.g. in the choice of evolution variable. Here, we recall but some pertinent features, which are relevant for the subsequent discussion of medium effects. We do this by focussing on one particular MC implementation, the mass-ordered parton shower used e.g. in the PYTHIA 6.4 event generator [22]. For each parton  $a$  in a parton shower, the kinematics of its branching  $a \rightarrow b + c$  is given in terms of the virtuality of the parent parton and the momentum fraction  $z$  of its total energy, which is carried by one of its daughters. The probability that no splitting occurs between an initial and final virtuality  $Q_i$  and  $Q_f$ , respectively, is described by the Sudakov factor

$$S_a(Q_i^2, Q_f^2) = \exp \left[ - \int_{Q_f^2}^{Q_i^2} \frac{dQ'^2}{Q'^2} \int_{z_-(Q'^2, E)}^{z_+(Q'^2, E)} dz \frac{\alpha_s(z(1-z)Q'^2)}{2\pi} \sum_{b,c} \hat{P}_{a \rightarrow bc}(z) \right]. \quad (4.37)$$

Here,  $\hat{P}_{a \rightarrow bc}(z)$  are the standard LO parton splitting functions for quarks and gluons ( $a, b, c \in \{q, g\}$ ). The  $z$ -integral must be regularized by an infrared cut-off scale below which parton splittings are considered to be not resolvable. This defines  $z_+$ ,  $z_-$ . The probability density  $\Sigma_a(Q_i^2, Q^2)$  for a splitting to occur at virtuality  $Q^2$  is given in terms of the no-splitting probability (4.37) as

$$\Sigma_a(Q_i^2, Q^2) = \frac{dS_a(Q_i^2, Q^2)}{d(\ln Q^2)} = S_a(Q_i^2, Q^2) \sum_{b,c} \int_{z_-(Q^2, E)}^{z_+(Q^2, E)} dz \frac{\alpha_s(z(1-z)Q^2)}{2\pi} \hat{P}_{a \rightarrow bc}(z). \quad (4.38)$$

Here, the Sudakov form factor  $S_a(Q_i^2, Q^2)$  denotes the probability for evolving from  $Q_i^2$  to  $Q^2$  without splitting, and the remaining factor is the differential probability for the splitting  $a \rightarrow b + c$  at  $Q^2$ , summed over all  $b$  and  $c$ .

To be specific: In this case, the parton shower for a parent parton  $a$  of energy  $E$  is initiated by determining its virtuality  $Q_a^2$  according to the probability density  $\Sigma_a(E^2, Q^2)$ . In accordance with (4.38), one then selects the type of parton splitting, and the momentum fractions of the daughters within the kinematically allowed range  $z \in [z_-(Q_a^2, E), z_+(Q_a^2, E)]$ . Then, one specifies the virtualities  $Q_b$ ,  $Q_c$  of the daughters subject to some constraints: the virtuality should lie in between a hadronization scale

and the energy of the daughter, and the virtualities of the daughters should satisfy  $Q_b^2 + Q_c^2 < Q_a^2$ . This branching is accepted if the momentum fraction  $z$  chosen initially lie within the kinematically allowed range for daughter masses  $Q_b, Q_c$ . Otherwise, new values for  $Q_b, Q_c$  are chosen. If the branching is accepted, one reconstructs the full four-momentum for both daughters. Then, one treats them as seeds for subsequent branching processes. The partonic branching is terminated with the probability  $S_a(Q_i^2, Q_0^2)$  that no further branching occurs up to the hadronization scale  $Q_0$ .

Implementing exact angular ordering in the parton shower is important to ensure MLLA accuracy, see section 2.3.3. In the specific MC implementation discussed above, this can be achieved by rejecting the generated  $z$ -values if angular ordering is not satisfied. In other MC algorithms, which use different ordering variables, this implementation of angular ordering is achieved differently.

From the above, it should be clear that any MC algorithm of jet quenching amounts primarily to specifying how the no-splitting probability (4.37) and the probability density (4.38) for branching can be supplemented by medium effects.

#### 4.4.2 Simulating elastic interactions

Elastic interactions, in which the parton exchanges momentum and color with the medium, can be modeled incoherently. In general, one can assume a density  $n$  with which such elastic interactions occur along the path of the parton projectile, and an elastic cross section  $\sigma_{\text{el}}$ , which determines the kinematics of the interaction. In close analogy to the Sudakov factor (4.37), one defines [36] then the probability that no scattering occurs within a time interval  $\tau$

$$S_{\text{no scatt}}(\tau) = \exp[-\sigma_{\text{el}} n \tau \beta], \quad (4.39)$$

where  $\beta$  denotes the velocity of the parton and the density  $n$  can be a function of the traveled distance  $\beta\tau$ . If the time  $\tau$  is specified to be the lifetime of a virtual parton prior to subsequent branching,  $\tau \sim E/Q^2$ , then (4.39) specifies the probability that this subsequent branching occurs without prior interaction with the medium. With the probability  $[1 - S_{\text{no scatt}}(\tau)]$ , the parton scatters at some time  $\tau' < \tau$ . In this case, the parton exchanges momentum with a scattering centre according to the differential elastic cross section specified by the model. For instance, this could be the suitably regularized, leading perturbative  $t$ -channel exchange term for quark-quark ( $C_R = 4/9$ ), quark-gluon ( $C_R = 1$ ) and gluon-gluon ( $C_R = 9/4$ ) scattering

$$\frac{d\sigma_{\text{el}}}{d|t|} = \frac{\pi\alpha_s^2}{s^2} C_R \frac{s^2 + u^2}{|t|^2} \Big|_{\text{regularised}}. \quad (4.40)$$

Multiple elastic scattering is implemented by specifying the momentum of the outgoing partons from  $d\sigma_{\text{el}}$  and further propagating them according to (4.39).

This prescription interpolates between two controlled limiting cases: First, in the absence of a medium, one recovers the benchmark results of a vacuum parton shower. Second, in the case that many elastic interactions occur within the lifetime of a virtual parton, vacuum branching processes become unimportant and the code reproduces the results of analytic collisional energy loss calculations, described in section 4.3. In addition, this MC technique provides easy access to information about the dynamical fluctuations around the event average, and to information about multi-particle final states, such as distributions of recoil particles.

#### 4.4.3 Simulating inelastic processes

MC implementations of medium-induced parton energy loss started in the early 90's with HIJING [114], which simulates complete nucleus-nucleus collisions and includes a simplified model for radiative energy loss. More recently, there have been several developments: there is PYQUEN [115], which modifies *a posteriori* the standard PYTHIA 6.2 jet events essentially by reducing the energy of partons in the shower

and by adding additional gluons to that shower according to distributions motivated by parton energy loss calculations. The first version of the final state parton shower JEWEL [36] implements elastic energy loss as described in section 4.4.2 and it mimics radiative energy loss by multiplying the vacuum splitting function in the parton shower with a factor  $(1 + f_{\text{med}})$  [40]. A future version of JEWEL will simulate medium-induced radiation by an algorithm based on formation time, which is known to account for non-abelian quantum interference as described in the context of equation (4.42) below [119]. Q-PYTHIA [116] simulates medium-modifications of a final state parton shower by modifying the splitting functions in a PYTHIA vacuum shower as described below. There is also a model YAJEM (Yet Another Jet Energy-loss Model), where the virtuality of partons in the shower is increased due to interactions with the medium thus stimulating additional gluon emissions [117]. This implements a conceivable microscopic dynamics which is not yet supported by analytical calculations. There is a recent comparison study of several medium-modified QCD evolution shower scenarios [118].

In this section, we focus mainly on MC algorithms which

1. aim at simulating the medium-modification of the entire parton fragmentation pattern rather than focussing on the energy degradation of the most energetic partons only. In particular, the MC algorithm should reduce to a phenomenologically viable vacuum parton shower in the absence of medium effects.
2. aim at a dynamical MC implementation of the analytical results of medium-induced gluon radiation reviewed in section 4.2.

Two different methods of simulating medium-modified parton showers aim at satisfying these criteria:

**The method of medium-modified splitting functions** Inelastic interactions between projectile and the medium may be regarded as a source of an additional medium-induced branching  $a \rightarrow b + c$  of the projectile parton  $a$ . For instance, within the BDMPS formalism for parton energy loss, medium-induced gluon radiation can be written formally as a modification of the vacuum splitting function, see e.g. equation (4.30) and subsequent discussion. This motivates an approach, in which the splitting function  $\hat{P}_{a \rightarrow bc}(z)$  in the vacuum parton shower defined by (4.35), (4.36) is replaced by a medium-modified splitting function

$$\hat{P}_{a \rightarrow bc}(z)^{\text{tot}} = \hat{P}_{a \rightarrow bc}(z)^{\text{vac}} + \Delta \hat{P}_{a \rightarrow bc}(z, Q^2, \hat{q}, L, E). \quad (4.41)$$

The MC model Q-PYTHIA [116] follows this approach and it specifies the medium-modification  $\Delta \hat{P}_{a \rightarrow bc}(z, Q^2, \hat{q}, L, E)$  of the parton branching in terms of the analytically known gluon energy distribution  $\omega dI/d\omega$ . As such, the medium-modification in (4.41) does not depend solely on the momentum fraction  $z$ , but it depends also on the in-medium path length  $L$ , the energy of the projectile  $E$ , properties of the medium which we characterize here by the quenching parameter  $\hat{q}$  and the virtuality  $Q^2$  of the projectile quark. The current version of Q-PYTHIA aims at taking coherence effects into account by attributing the coherence time (2.5) to the radiated gluon and calculating subsequent medium-induced gluon emissions for a reduced in-medium path length  $L - l_{\text{coh}}$ , where  $l_{\text{coh}} = 2\omega/k_T^2$ . In this way, Q-PYTHIA is automatically consistent with the vacuum baseline in the absence of a medium, and it reproduces the analytically known results for the medium-modification of the single gluon energy distribution. Moreover, this proposal has the advantage that the replacement (4.41) is relatively easy to implement in existing event generators. On the other hand, the prescription (4.41) does not allow to follow dynamically the recoil from the projectile parton to the medium - this may be important e.g. for the description of the soft particle yield associated to highly energetic jets. A more fundamental problem can be understood by recalling that a typical parton shower will also include gluons, which are fully formed in the sense of independent quanta, well before the partonic projectile has traversed the entire medium. The splitting function of such a gluon should not depend on the maximal remaining in-medium path length  $L - l_{\text{coh}}$ , simply since the gluon production process is completed before the gluon "sees" this length. This shows that Q-PYTHIA remains, strictly speaking, a heuristic proposal, although it encodes much of what is known analytically about radiative parton energy loss.

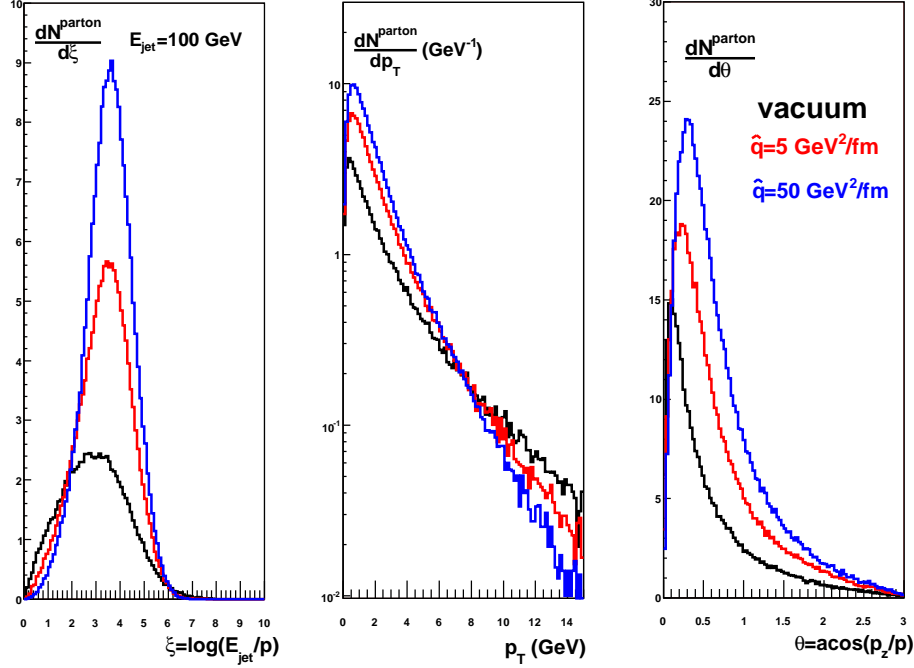


Figure 6: Results of the Q-PYTHIA MC final state parton shower for the intrajet parton distributions in  $\xi = \ln(E_{\text{jet}}/p)$  (left),  $p_T$  (middle) and  $\theta = \arccos(p_z/p)$  (right) of a gluon jet with energy  $E_{\text{jet}} = 100$  GeV. The vacuum baseline is compared to a medium of length  $L = 2$  with transport coefficient  $\hat{q} = 5$  and  $50 \text{ GeV}^2/\text{fm}$ . Figure taken from Ref. [116].

**Probabilistic implementation of non-abelian quantum interference** If the time between subsequent interactions of a partonic projectile and the medium is much larger than the formation time (2.5) of the gluon produced in an inelastic process, then this inelastic process is an incoherent gluon production, which can be iterated probabilistically. The challenge for any probabilistic MC implementation of the medium-dependence of inelastic processes is the opposite case that the gluon formation process extends over more than one interaction between projectile and medium. Then, spatially separated interactions act coherently and quantum interference becomes important for gluon production. It has been demonstrated [119] that this quantum interference can be implemented in a probabilistic MC algorithm by requiring that the momentum transfer from different scattering centers to the partonic projectile acts totally coherently for gluon production, if it occurs within the formation time  $t_f$ , and that it acts incoherently, if it occurs outside  $t_f$ .

The proposed MC algorithm is as follows [119]: To be specific, consider a medium, characterized by a distribution of target scattering centers  $Q_T$ , which present inelastic  $\sigma^{qQ_T \rightarrow qQ_T g}$  and elastic  $\sigma^{qQ_T \rightarrow qQ_T}$  cross sections to a projectile  $q$ . Consider the case that the MC algorithm specifies that a particular scattering center  $Q_T$  is involved in an inelastic process. If the initial formation time

$$t_f = 2\omega/\mathbf{k}_{\text{init}}^2 \quad (4.42)$$

of that gluon is shorter than the distance to the next scattering center, then the gluon is formed in this interaction. The outgoing gluon and quark are propagated further as independent degrees of freedom. In the opposite case, the projectile components emerging from the first interaction will interact a second time before the gluon is formed. At this second interaction, production of an additional gluon is not possible, since it interferes destructively with the not yet fully formed gluon. So, the second scattering center is the source of an elastic interaction of transverse momentum  $q_T$  transferred to the projectile components.

The MC algorithm adds  $q_T$  to the transverse momentum of the first interaction and it recalculates the inelastic gluon production under the assumption that both scattering centers act effectively as one coherent scattering center. In practice, this increases the transverse momentum between the outgoing quark and gluon to  $\mathbf{k}_{\text{init}} \rightarrow \mathbf{k}_{\text{init}} + \mathbf{q}$ , and hence it shortens the formation time to

$$t'_f = 2\omega / (\mathbf{k}_{\text{init}} + \mathbf{q})^2 . \quad (4.43)$$

If this shortened formation time  $t'_f$  is shorter than the distance to the next (third) scattering, then the gluon is regarded as fully formed. Otherwise, the procedure is repeated and the elastic momentum transfer of this next scattering center is added to  $k_{\perp\text{init}} + q_T$ .

The above procedure provides a probabilistic implementation of (4.12). This can be seen very clearly on the level of the  $N = 1$  opacity expansion: Expressing the initial transverse gluon momentum  $\mathbf{k}_{\text{init}}$  in terms of the outgoing transverse gluon momentum  $\mathbf{k}_{\text{init}} = \mathbf{k} - \mathbf{q}$ , one finds that the gluon formation times  $t_f, t'_f$  prior to and after secondary scattering correspond exactly to the formation times  $\tau_1, \tau$  in the  $N = 1$  opacity result (4.15). In particular, the interference term  $[L/\tau_1 - \sin L/\tau_1]$  in (4.15) prevents gluons from being radiated prior to interacting at distance  $L$ , if their formation time is too long. This is exactly the coherence condition in the MC algorithm described above.

The algorithm described here is consistent with what is known qualitatively and quantitatively about medium-induced gluon radiation (4.12). In particular, it reproduces the  $L^2$ -dependence of the average energy loss (4.25) and the characteristic  $\sqrt{\omega}$ -modification of the gluon energy distribution in the limit of multiple soft scatterings. The present author expects that the same formation time physics can account reliably for multi-gluon emission. However, very little is known about the medium-modification of multi-gluon emissions and, strictly speaking, the algorithm remains at present a credible but heuristic extrapolation to this case.

#### 4.5 Applying the AdS/CFT correspondence to in-medium parton propagation

The evolution of a parton shower is a weak coupling phenomenon as long as the virtuality of partons lies well above the hadronic scale. In fact, irrespective of whether parton splitting occurs in the vacuum or in the medium, one expects the coupling at the splitting vertex to be perturbatively small if the virtuality of the parent parton is sufficiently high. However, the interaction between components of the parton shower and the medium may involve multiple soft momentum exchanges, which may occur with non-perturbatively large coupling. This motivates the application of strong coupling techniques to in-medium parton propagation.

Finite temperature lattice QCD has been the main calculational tool for first principle calculations of medium properties at non-perturbatively large coupling [120]. However, information on real-time dynamics in a strongly coupled quark gluon plasma is difficult to extract from lattice QCD. For a large class of non-abelian thermal gauge theories, the Anti-de Sitter / Conformal Field Theory (AdS/CFT) conjecture offers an alternative. The AdS/CFT conjecture asserts that in the limit of large number of colors ( $N_c$ ) and large 't Hooft coupling  $\lambda = g^2 N_c$ , a certain class of non-abelian gauge field theories is equivalent to the supergravity limit of a corresponding dual string theory, with the background metric describing a curved five-dimensional anti-deSitter space, see Ref. [121] for a review of the original literature. This AdS/CFT correspondence also applies to the thermal sector, if the five-dimensional anti-deSitter space is endowed with a Schwarzschild black hole. In practice, the AdS/CFT correspondence provides a technique for doing complicated or otherwise intractable calculations in the strong coupling limit of a quantum field theory by solving a comparatively simpler semi-classical problem in the dual gravity theory.

The gravity dual of QCD is not known. One may identify two main motivations for applying the AdS/CFT correspondence to problems in heavy ion physics. First, on a qualitative level, there are open conceptual issues in QCD for which one may want to seek guidance in other non-abelian field

theories for which strong coupling techniques exist. For instance, the strongly coupled plasmas described by AdS/CFT are known to be free of quasi-particles, and the picture of the QCD plasma as a system of weakly coupled quasi-particles is on unclear footing, but most derivations of QCD transport and hydrodynamics rest on it. Here, the AdS/CFT correspondence can shed light on the conceptual issue, which features of transport theory persist beyond the quasi-particle picture. Second, on a quantitative level, applications of the AdS/CFT correspondence to QCD must ultimately involve an argument that what has been calculated for a large class of non-abelian quantum field theories with gravity dual (which share many features with QCD), can be used as guidance for QCD. This assumption is supported by several observations. For instance, the energy density and pressure, calculated with the help of the AdS/CFT correspondence, is three quarters of the Stefan-Boltzmann value in the limit of infinitely strong coupling [122] and it is slightly larger for large but finite  $\lambda$ , in good agreement with the value found in QCD lattice calculations for temperatures above but at the order of the critical temperature  $T_c$ . Another well-known example is the calculation of the ratio  $\eta/s$  of shear viscosity over entropy density [123]. This quantity turns out to take the same universal and extremely low value  $1/4\pi$  in the strong coupling limit of all quantum field theories with a gravity dual. On the one hand, the universality of this result may be taken as an indication that the value of  $\eta/s$  in a QCD plasma is also very low. This assumption is supported by first exploratory lattice calculations [124], and it is in line with hydrodynamical simulations of RHIC data. These and other examples have prompted in recent years applications of the AdS/CFT correspondence to the calculation of many quantities, which are of phenomenological interest for heavy ion physics. Here, we focus solely on two conceptually different approaches to studying parton energy loss with the help of the AdS/CFT correspondence:

**Calculation of the quenching parameter** [125] This approach does not aim at applying strong coupling techniques to all aspects of in-medium parton propagation. Rather, it takes into account that at sufficiently high virtuality, parton branching in QCD is best described perturbatively. In the multiple soft scattering limit, the only non-perturbative input to the medium-induced gluon energy distribution (4.12) is the quenching parameter  $\hat{q}$ , which is defined as the short distance behavior of a light-like Wilson loop,

$$\langle W^A(\mathcal{C}_{\text{light-like}}) \rangle = \exp \left[ -\frac{1}{4\sqrt{2}} \hat{q} L^- r^2 \right]. \quad (4.44)$$

Here,  $\mathcal{C}_{\text{light-like}}$  denotes a closed path, consisting of two very long parallel pieces of length  $L^-$  along the light cone, which are separated by the transverse distance  $r$ . As explained in detail in Ref. [126], this definition follows from the observation that in the high energy limit, the path integral (4.11) reduces to (4.44). For the  $\mathcal{N} = 4$  super-symmetric Yang Mills (SYM) theory, the result for large 't Hooft coupling  $\lambda = g^2 N_c$  has been calculated by use of the AdS/CFT correspondence [126]

$$\hat{q}_{SYM} = \frac{\pi^{3/2} \Gamma(3/4)}{\Gamma(5/4)} \sqrt{\lambda} T^3 \approx 26.69 \sqrt{\alpha_{SYM} N_c} T^3. \quad (4.45)$$

If one would relate this to QCD by fixing  $N_c = 3$  and  $\alpha_{SYM} = .5$ , then  $\hat{q}_{SYM} = 4.4 \text{ GeV}^2/\text{fm}$  for a temperature of  $T = 300 \text{ MeV}$ . This number is comparable to the values extracted in comparisons of jet quenching models to RHIC data. For different theories with gravity dual, one finds that the quenching parameter scales with the square root of the entropy density [125]. If QCD follows this behavior, then  $\hat{q}_{QCD}/\hat{q}_{SYM} = \sqrt{47.5/120} \approx 0.63$ . Moreover,

$$\hat{q}_{LHC} = \sqrt{\frac{dN_{\text{ch}}^{\text{LHC}}/d\eta}{dN_{\text{ch}}^{\text{RHIC}}/d\eta}} \hat{q}_{\text{RHIC}}. \quad (4.46)$$

Other calculations of the quenching parameter  $\hat{q}$ , and their relation to observations at RHIC are discussed in Ref. [126].

**Drag calculations of parton energy loss** [127–129] This approach applies the AdS/CFT strong coupling technique to all aspects of in-medium parton energy loss. One considers a heavy quark of velocity  $v$  and

one calculates the force needed to maintain this velocity, that is, the force needed to drag the quark through the medium at velocity  $v$ . This allows one to determine the medium-induced energy loss of the quark at velocity  $v$ ,

$$\frac{dE}{dx} = -\frac{\pi}{2} \sqrt{\lambda} T^2 \frac{v}{\sqrt{1-v^2}}. \quad (4.47)$$

We remark that the derivation of (4.47) is valid for sufficiently low velocities,

$$\sqrt{\gamma} < \frac{M}{\sqrt{\lambda} T}, \quad (4.48)$$

while the derivation of the quenching parameter is valid only in the opposite limit of sufficiently small quark masses  $M$  or sufficiently high parton velocities, when  $\sqrt{\gamma} > \frac{M}{\sqrt{\lambda} T}$ . This is one of the reason which has made the comparison of drag calculations and calculations of the quenching parameter difficult. Arguments have been put forward that for velocities exceeding (4.48), the drag result (4.47) will be small compared to energy loss due to acceleration [130, 131]. In a particular toy model, energy loss due to radiation of an accelerated quark was shown to interfere destructively with energy loss due to drag [131]. The velocity dependence of the drag result (4.47) is characteristically different from that of QCD. However, based on a heuristic interpretation of (4.47) in terms of a quasi-particle picture, one has argued for a close analogy of the drag result and the QCD result for radiative parton energy loss [132].

In contrast to calculations of the quenching parameter, drag calculations of parton energy loss provide a complete dynamical description of parton energy loss, assuming the same non-perturbatively large coupling constant to all stages of the problem. While this treatment neglects the scale-dependence of the QCD coupling constant, it has the advantage that the interaction between partonic projectile and medium can be formulated without any further model assumption. Dragged quarks are well-defined sources of hydrodynamic perturbations in non-abelian plasmas. In particular, one finds that at least some fraction of the energy, deposited by a dragged quark in the medium, propagates via sound waves and gives rise to a Mach cone [133]. A lot of work on the radiation pattern associated with dragged quarks has been motivated by suggestions that this Mach cone like structure survives hadronization and that it may have been observed already at RHIC in the angular dependence of high- $p_T$  triggered two-particle correlations.

## References

- [1] C. Amsler *et al.* [Particle Data Group], Phys. Lett. B **667**, 1 (2008).
- [2] R. Baier, D. Schiff and B. G. Zakharov, Ann. Rev. Nucl. Part. Sci. **50** (2000) 37 [arXiv:hep-ph/0002198].
- [3] A. Kovner and U. A. Wiedemann, arXiv:hep-ph/0304151.
- [4] M. Gyulassy, I. Vitev, X. N. Wang and B. W. Zhang, arXiv:nucl-th/0302077.
- [5] P. Jacobs and X. N. Wang, Prog. Part. Nucl. Phys. **54** (2005) 443 [arXiv:hep-ph/0405125].
- [6] J. Casalderrey-Solana and C. A. Salgado, Acta Phys. Polon. B **38** (2007) 3731 [arXiv:0712.3443 [hep-ph]].
- [7] D. d’Enterria, arXiv:0902.2011 [nucl-ex].
- [8] I. Arsene *et al.* [BRAHMS Collaboration], Nucl. Phys. A **757** (2005) 1;
- [9] K. Adcox *et al.* [PHENIX Collaboration], Nucl. Phys. A **757** (2005) 184;
- [10] B. B. Back *et al.* [PHOBOS Collaboration], Nucl. Phys. A **757** (2005) 28;

- [11] J. Adams *et al.* [STAR Collaboration], Nucl. Phys. A **757** (2005) 102.
- [12] F. Carminati *et al.* [ALICE Collaboration], J. Phys. G **30** (2004) 1517.
- [13] B. Alessandro *et al.* [ALICE Collaboration], J. Phys. G **32** (2006) 1295.
- [14] D. d’Enterria *et al.* [CMS Collaboration], J. Phys. G **34** (2007) 2307.
- [15] A. H. . Mueller, *SINGAPORE, SINGAPORE: WORLD SCIENTIFIC (1989) 614 P. (ADVANCED SERIES ON DIRECTIONS IN HIGH ENERGY PHYSICS, 5)*
- [16] R. K. Ellis, W. J. Stirling and B. R. Webber, Camb. Monogr. Part. Phys. Nucl. Phys. Cosmol. **8** (1996) 1.
- [17] G. Sterman, *Cambridge, UK: Univ. Pr. (1993) 572 p*
- [18] M. Luo, J. w. Qiu and G. Sterman, Phys. Rev. D **50** (1994) 1951.
- [19] M. Luo, J. w. Qiu and G. Sterman, Phys. Rev. D **49** (1994) 4493.
- [20] X. N. Wang, Phys. Lett. B **579** (2004) 299 [arXiv:nucl-th/0307036].
- [21] Y. L. Dokshitzer, V. A. Khoze, A. H. Mueller and S. I. Troian, *Gif-sur-Yvette, France: Ed. Frontieres (1991) 274 p. (Basics of)*
- [22] T. Sjostrand, S. Mrenna and P. Skands, JHEP **0605** (2006) 026 [arXiv:hep-ph/0603175].
- [23] G. Corcella *et al.*, JHEP **0101** (2001) 010 [arXiv:hep-ph/0011363].
- [24] T. Gleisberg, S. Hoche, F. Krauss, A. Schaliche, S. Schumann and J. C. Winter, JHEP **0402** (2004) 056 [arXiv:hep-ph/0311263].
- [25] J.E. Huth *et al.*, FERMILAB-CONF-90-249-E (1990).
- [26] G. Soyez, arXiv:0812.2362 [hep-ph].
- [27] S. Salur [STAR Collaboration], arXiv:0809.1609 [nucl-ex].
- [28] G. P. Salam and G. Soyez, JHEP **0705** (2007) 086 [arXiv:0704.0292 [hep-ph]].
- [29] B. Abbott, M. Bhattacharjee, D. Elvira, F. Nang and H. Weerts [D0 Coll.], FERMILAB-PUB-97-242-E
- [30] Y. L. Dokshitzer, G. D. Leder, S. Moretti and B. R. Webber, JHEP **9708** (1997) 001 [arXiv:hep-ph/9707323].
- [31] M. Wobisch and T. Wengler, arXiv:hep-ph/9907280.
- [32] S. Catani, Y. L. Dokshitzer, M. H. Seymour and B. R. Webber, Nucl. Phys. B **406** (1993) 187.
- [33] M. Cacciari, G. P. Salam and G. Soyez, JHEP **0804** (2008) 063 [arXiv:0802.1189 [hep-ph]].
- [34] S. Catani, Y. L. Dokshitzer, M. Olsson, G. Turnock and B. R. Webber, Phys. Lett. B **269** (1991) 432.
- [35] A. Heister *et al.* [ALEPH Collaboration], Eur. Phys. J. C **35** (2004) 457.
- [36] K. Zapp, G. Ingelman, J. Rathsman, J. Stachel and U. A. Wiedemann, arXiv:0804.3568 [hep-ph].



- [37] Y. L. Dokshitzer, V. A. Khoze and S. I. Troian, *Adv. Ser. Direct. High Energy Phys.* **5** (1988) 241.
- [38] C. P. Fong and B. R. Webber, *Nucl. Phys. B* **355** (1991) 54.
- [39] Y. I. Azimov, Y. L. Dokshitzer, V. A. Khoze and S. I. Troian, *Z. Phys. C* **27** (1985) 65.
- [40] N. Borghini and U. A. Wiedemann, arXiv:hep-ph/0506218.
- [41] R. P. Ramos, *JHEP* **0606** (2006) 019 [arXiv:hep-ph/0605083].
- [42] F. Arleo, R. P. Ramos and B. Machet, *Phys. Rev. Lett.* **100** (2008) 052002 [arXiv:0707.3391 [hep-ph]].
- [43] S. Sapeta and U. A. Wiedemann, arXiv:0809.4251 [hep-ph].
- [44] P. Braun-Munzinger, K. Redlich and J. Stachel, arXiv:nucl-th/0304013.
- [45] B. I. Abelev *et al.* [STAR Collaboration], *Phys. Rev. Lett.* **97**, 152301 (2006) [arXiv:nucl-ex/0606003].
- [46] S. Sapeta and U. A. Wiedemann, *Eur. Phys. J. C* **55** (2008) 293 [arXiv:0707.3494 [hep-ph]].
- [47] R. Baier, Y. L. Dokshitzer, A. H. Mueller and D. Schiff, *JHEP* **0109**, 033 (2001) [arXiv:hep-ph/0106347].
- [48] B. Muller, *Phys. Rev. C* **67** (2003) 061901 [arXiv:nucl-th/0208038].
- [49] K. J. Eskola, H. Honkanen, C. A. Salgado and U. A. Wiedemann, *Nucl. Phys. A* **747** (2005) 511 [arXiv:hep-ph/0406319].
- [50] S. S. Adler *et al.* [PHENIX Collaboration], *Phys. Rev. Lett.* **94**, 232301 (2005) [arXiv:nucl-ex/0503003].
- [51] A. Dainese, C. Loizides and G. Paic, *Eur. Phys. J. C* **38** (2005) 461 [arXiv:hep-ph/0406201].
- [52] T. Renk, *Phys. Rev. C* **77** (2008) 017901 [arXiv:0711.1030 [hep-ph]].
- [53] S. A. Bass, C. Gale, A. Majumder, C. Nonaka, G. Y. Qin, T. Renk and J. Ruppert, arXiv:0808.0908 [nucl-th].
- [54] S. Wicks, W. Horowitz, M. Djordjevic and M. Gyulassy, *Nucl. Phys. A* **784** (2007) 426 [arXiv:nucl-th/0512076].
- [55] TECHQM Main Page, [https://wiki.bnl.gov/TECHQM/index.php/Main\\_Page](https://wiki.bnl.gov/TECHQM/index.php/Main_Page)
- [56] C. Adler *et al.* [STAR Collaboration], *Phys. Rev. Lett.* **90** (2003) 082302 [arXiv:nucl-ex/0210033].
- [57] J. Adams *et al.* [STAR Collaboration], *Phys. Rev. Lett.* **97** (2006) 162301 [arXiv:nucl-ex/0604018].
- [58] C. Loizides, *Eur. Phys. J. C* **49** (2007) 339 [arXiv:hep-ph/0608133].
- [59] A. Majumder and X. N. Wang, *Phys. Rev. D* **70** (2004) 014007 [arXiv:hep-ph/0402245].
- [60] A. Majumder and X. N. Wang, *Phys. Rev. D* **72** (2005) 034007 [arXiv:hep-ph/0411174].
- [61] X. N. Wang, Z. Huang and I. Sarcevic, *Phys. Rev. Lett.* **77** (1996) 231 [arXiv:hep-ph/9605213].

- [62] F. Arleo, P. Aurenche, Z. Belghobsi and J. P. Guillet, JHEP **0411** (2004) 009 [arXiv:hep-ph/0410088].
- [63] F. Arleo, JHEP **0609** (2006) 015 [arXiv:hep-ph/0601075].
- [64] C. A. Salgado and U. A. Wiedemann, Phys. Rev. Lett. **93** (2004) 042301 [arXiv:hep-ph/0310079].
- [65] A. D. Polosa and C. A. Salgado, Phys. Rev. C **75** (2007) 041901 [arXiv:hep-ph/0607295].
- [66] N. Armesto, C. A. Salgado and U. A. Wiedemann, Phys. Rev. Lett. **93** (2004) 242301 [arXiv:hep-ph/0405301].
- [67] J. Casalderrey-Solana, E. V. Shuryak and D. Teaney, arXiv:hep-ph/0602183.
- [68] J. Casalderrey-Solana, E. V. Shuryak and D. Teaney, J. Phys. Conf. Ser. **27**, 22 (2005) [Nucl. Phys. A **774**, 577 (2006)] [arXiv:hep-ph/0411315].
- [69] G. Arnison *et al.* [UA1 Collaboration], Phys. Lett. B **132** (1983) 214.
- [70] S. A. Voloshin, Phys. Lett. B **632** (2006) 490 [arXiv:nucl-th/0312065].
- [71] A. Kovner and U. A. Wiedemann, Phys. Rev. D **64** (2001) 114002 [arXiv:hep-ph/0106240].
- [72] B. Z. Kopeliovich, A. V. Tarasov and A. Schafer, Phys. Rev. C **59**, 1609 (1999) [arXiv:hep-ph/9808378].
- [73] B. G. Zakharov, JETP Lett. **63** (1996) 952 [arXiv:hep-ph/9607440].
- [74] B. G. Zakharov, JETP Lett. **65** (1997) 615 [arXiv:hep-ph/9704255].
- [75] B. G. Zakharov, Phys. Atom. Nucl. **61** (1998) 838 [Yad. Fiz. **61** (1998) 924] [arXiv:hep-ph/9807540].
- [76] U. A. Wiedemann and M. Gyulassy, Nucl. Phys. B **560**, 345 (1999) [arXiv:hep-ph/9906257].
- [77] U. A. Wiedemann, Nucl. Phys. B **588** (2000) 303.
- [78] M. Gyulassy, P. Levai and I. Vitev, Nucl. Phys. B **594** (2001) 371.
- [79] M. Gyulassy and X. N. Wang, Nucl. Phys. B **420** (1994) 583.
- [80] P. Arnold, arXiv:0808.2767 [hep-ph].
- [81] U. A. Wiedemann, Nucl. Phys. A **690**, 731 (2001) [arXiv:hep-ph/0008241].
- [82] R. Baier, Y. L. Dokshitzer, A. H. Mueller, S. Peigne and D. Schiff, Nucl. Phys. B **483**, 291 (1997) [arXiv:hep-ph/9607355].
- [83] R. Baier, Y. L. Dokshitzer, A. H. Mueller, S. Peigné and D. Schiff, Nucl. Phys. B **484** (1997) 265.
- [84] R. Baier, Y. L. Dokshitzer, A. H. Mueller and D. Schiff, Phys. Rev. C **58** (1998) 1706 [arXiv:hep-ph/9803473].
- [85] C. A. Salgado and U. A. Wiedemann, Phys. Rev. Lett. **89** (2002) 092303 [arXiv:hep-ph/0204221].
- [86] C. A. Salgado and U. A. Wiedemann, Phys. Rev. D **68** (2003) 014008 [arXiv:hep-ph/0302184].
- [87] Y. L. Dokshitzer and D. E. Kharzeev, Phys. Lett. B **519** (2001) 199.

- [88] N. Armesto, C. A. Salgado and U. A. Wiedemann, *Phys. Rev. D* **69** (2004) 114003.
- [89] B. W. Zhang, E. Wang and X. N. Wang, *Phys. Rev. Lett.* **93** (2004) 072301.
- [90] M. Djordjevic and M. Gyulassy, *Nucl. Phys. A* **733** (2004) 265.
- [91] N. Armesto, A. Dainese, C. A. Salgado and U. A. Wiedemann, *Phys. Rev. D* **71** (2005) 054027.
- [92] M. Djordjevic, M. Gyulassy, R. Vogt and S. Wicks, *Phys. Lett. B* **632** (2006) 81 [arXiv:nucl-th/0507019].
- [93] R. Rapp, arXiv:0812.3850 [hep-ph].
- [94] M. Gyulassy, P. Levai and I. Vitev, *Phys. Lett. B* **538** (2002) 282 [arXiv:nucl-th/0112071].
- [95] X. F. Guo and X. N. Wang, *Phys. Rev. Lett.* **85** (2000) 3591 [arXiv:hep-ph/0005044].
- [96] J. A. Osborne, E. Wang and X. N. Wang, arXiv:hep-ph/0212131.
- [97] N. Armesto, L. Cunqueiro, C. A. Salgado and W. C. Xiang, *JHEP* **0802** (2008) 048 [arXiv:0710.3073 [hep-ph]].
- [98] S. Domdey, G. Ingelman, H. J. Pirner, J. Rathsman, J. Stachel and K. Zapp, arXiv:0802.3282 [hep-ph].
- [99] X. N. Wang and X. F. Guo, *Nucl. Phys. A* **696** (2001) 788.
- [100] X. N. Wang and X. f. Guo, *Nucl. Phys. A* **696** (2001) 788 [arXiv:hep-ph/0102230].
- [101] P. Arnold, G. D. Moore and L. G. Yaffe, *JHEP* **0206** (2002) 030 [arXiv:hep-ph/0204343].
- [102] J. D. Bjorken, *preprint Fermilab-pub-82-059-thy*.
- [103] M. H. Thoma and M. Gyulassy, *Nucl. Phys. B* **351** (1991) 491.
- [104] E. Braaten and M. H. Thoma, *Phys. Rev. D* **44** (1991) 2625.
- [105] M. Djordjevic, *Phys. Rev. C* **74** (2006) 064907 [arXiv:nucl-th/0603066].
- [106] A. Adil, M. Gyulassy, W. A. Horowitz and S. Wicks, *Phys. Rev. C* **75** (2007) 044906 [arXiv:nucl-th/0606010].
- [107] S. Peigné and A. Peshier, arXiv:0802.4364 [hep-ph].
- [108] S. Wicks and M. Gyulassy, *J. Phys. G* **34** (2007) S989 [arXiv:nucl-th/0701088].
- [109] A. Peshier, arXiv:hep-ph/0601119.
- [110] R. Kolevatov and U. A. Wiedemann, arXiv:0812.0270 [hep-ph].
- [111] K. Zapp, G. Ingelman, J. Rathsman and J. Stachel, *Phys. Lett. B* **637** (2006) 179 [arXiv:hep-ph/0512300].
- [112] W. Cassing, K. Gallmeister and C. Greiner, *Nucl. Phys. A* **735** (2004) 277 [arXiv:hep-ph/0311358].
- [113] K. Werner, *Nucl. Phys. Proc. Suppl.* **175-176** (2008) 81.
- [114] X. N. Wang and M. Gyulassy, *Phys. Rev. D* **44** (1991) 3501.

- [115] I. P. Lokhtin and A. M. Snigirev, Eur. Phys. J. C **45** (2006) 211 [arXiv:hep-ph/0506189].
- [116] N. Armesto, L. Cunqueiro and C. A. Salgado, arXiv:0809.4433 [hep-ph].
- [117] T. Renk, Phys. Rev. C **78** (2008) 034908 [arXiv:0806.0305 [hep-ph]].
- [118] T. Renk, arXiv:0901.2818 [hep-ph].
- [119] K. Zapp, J. Stachel and U. A. Wiedemann, arXiv:0812.3888 [hep-ph].
- [120] E. Laermann and O. Philipsen, Ann. Rev. Nucl. Part. Sci. **53**, 163 (2003) [arXiv:hep-ph/0303042].
- [121] O. Aharony, S. S. Gubser, J. M. Maldacena, H. Ooguri and Y. Oz, Phys. Rept. **323**, 183 (2000) [arXiv:hep-th/9905111].
- [122] S. S. Gubser, I. R. Klebanov and A. W. Peet, Phys. Rev. D **54** (1996) 3915 [arXiv:hep-th/9602135].
- [123] G. Policastro, D. T. Son and A. O. Starinets, Phys. Rev. Lett. **87**, 081601 (2001) [arXiv:hep-th/0104066].
- [124] H. B. Meyer, Phys. Rev. D **76** (2007) 101701 [arXiv:0704.1801 [hep-lat]].
- [125] H. Liu, K. Rajagopal and U. A. Wiedemann, Phys. Rev. Lett. **97** (2006) 182301.
- [126] H. Liu, K. Rajagopal and U. A. Wiedemann, JHEP **0703** (2007) 066.
- [127] C. P. Herzog, A. Karch, P. Kovtun, C. Kozcaz and L. G. Yaffe, JHEP **0607**, 013 (2006) [arXiv:hep-th/0605158].
- [128] S. S. Gubser, Phys. Rev. D **74**, 126005 (2006) [arXiv:hep-th/0605182].
- [129] J. Casalderrey-Solana and D. Teaney, Phys. Rev. D **74**, 085012 (2006) [arXiv:hep-ph/0605199].
- [130] D. E. Kharzeev, arXiv:0809.3000 [hep-ph].
- [131] K. B. Fadafan, H. Liu, K. Rajagopal and U. A. Wiedemann, arXiv:0809.2869 [hep-ph].
- [132] F. Dominguez, C. Marquet, A. H. Mueller, B. Wu and B. W. Xiao, Nucl. Phys. A **811** (2008) 197 [arXiv:0803.3234 [nucl-th]].
- [133] S. S. Gubser, S. S. Pufu and A. Yarom, Phys. Rev. Lett. **100** (2008) 012301 [arXiv:0706.4307 [hep-th]].